

IMPROVED LABORATORY TRANSITION PROBABILITIES FOR Gd II
AND APPLICATION TO THE GADOLINIUM ABUNDANCES OF THE
SUN AND THREE r -PROCESS RICH, METAL-POOR STARS

(short title: Gd Transition Probabilities and Abundances)

E. A. Den Hartog, J. E. Lawler

Department of Physics, University of Wisconsin, Madison, WI 53706;

eadenhar@wisc.edu, jelawler@wisc.edu

C. Sneden

Department of Astronomy and McDonald Observatory, University of Texas,
Austin, TX 78712; chris@verdi.as.utexas.edu

and J. J. Cowan

Department of Physics and Astronomy, University of Oklahoma, Norman, OK
73019; cowan@nhn.ou.edu

ABSTRACT

Radiative lifetimes, accurate to $\pm 5\%$, have been measured for 49 even-parity and 14 odd-parity levels of Gd II using laser-induced fluorescence. The lifetimes are combined with branching fractions measured using Fourier transform spectrometry to determine transition probabilities for 611 lines of Gd II. This work is the largest-scale laboratory study to date of Gd II transition probabilities and the first using a high performance Fourier transform spectrometer. This improved data set has been used to determine a new solar photospheric Gd abundance, $\log \varepsilon = 1.11 \pm 0.03$. Revised Gd abundances have also been derived for the r -process-rich metal-poor giant stars CS 22892-052, BD+17°3248, and HD 115444. The resulting Gd/Eu abundance ratios are in very good agreement with the solar-system r -process ratio. We have employed the increasingly accurate stellar abundance determinations, resulting in large part from the more precise laboratory atomic data, to predict directly the Solar System r -process elemental abundances for Gd, Sm, Ho and Nd. Our analysis of the stellar data suggests slightly higher recommended values for the r -process contribution and total Solar System values, consistent with the photospheric determinations, for the elements for Gd, Sm, and Ho.

Subject headings: atomic data — stars: abundances stars: Population II — Sun: abundances

1. INTRODUCTION

Rare Earth (RE) elements are among the most spectroscopically accessible of the neutron (n -) capture elements. Many transitions of singly ionized RE species appear in the spectrum of the Sun and in stars over a significant temperature range. This accessibility makes RE species useful in studies of heavy element nucleosynthesis. The needed observations in the form of high-resolution, high signal-to-noise (S/N) spectra on a variety of targets from very large ground-based telescopes and the Hubble Space Telescope are available. Old metal-poor Galactic halo stars are very attractive targets because they provide a fossil record of the chemical make-up of our Galaxy when it, and the Universe, were very young (e.g., Gratton & Sneden 1994; McWilliam et al. 1995; Cowan et al. 1995; Sneden et al. 1996, Ryan et al. 1996, Cayrel et al. 2004). Recent abundance determinations of heavy n -capture elements in very metal-poor stars have yielded new insights on the roles of the r (apid)- and s (low)-processes in the initial burst of Galactic nucleosynthesis. The results of this ongoing work are reshaping our understanding of the chemical evolution of the Galaxy.

Although these studies of nucleosynthesis are proceeding at a good pace, there is a constant need for improved laboratory data, especially atomic transition probabilities. The accessibility of RE spectra from an observational astronomer's viewpoint is not matched by tractability from a theoretical atomic physicist's viewpoint. The combination of an open f-shell with hundreds to thousands of low lying levels, a breakdown of Russell-Saunders coupling, substantial relativistic effects, and massive configuration interactions makes the calculation of *ab initio* atomic transition probabilities a formidable undertaking. The Liège group (e.g. Biémont & Quinet (2003)) has systematically applied the relativistic Hartree Fock method to calculate RE transition probabilities. Even with an intense theoretical effort on these complex spectra, it is essential to have some good measurements for comparison. Fortunately an efficient experimental approach has been developed. Many of the recent experimental studies of RE atomic transition probabilities have combined radiative lifetimes from laser induced fluorescence (LIF) measurements with emission branching fractions measured using a Fourier transform spectrometer (FTS). This approach to determining atomic transition probabilities in complex spectra has proved to be both efficient and quite reliable. Our recent work on Sm II is just one example, and many other studies on RE transition probabilities are cited in the first paragraph of our Sm II paper (Lawler et al. 2006, hereafter LDSC06).

Singly-ionized gadolinium is one of the remaining RE species in need of modern measurements, and it is the focus of this work. We report new LIF radiative lifetime measurements for 49 even-parity and 14 odd-parity levels, as well as absolute atomic transition probabilities for 611 lines of Gd II. Our lifetime measurements are in good agreement with earlier, but less extensive, LIF measurements. Our branching fraction measurements, in combination with the LIF lifetimes, yielded both a large set of transition probabilities and the first based on modern methods. This improved data set has been used to determine a new solar photospheric Gd abundance and revised Gd abundances for the

r-process-rich metal-poor giant stars CS 22892-052, BD+17°3248, and HD 115444. Implications of these abundance determinations are discussed.

2. RADIATIVE LIFETIME MEASUREMENTS

Radiative lifetimes of 49 even-parity and 14 odd-parity levels of Gd II have been measured using time-resolved laser-induced fluorescence (LIF) on an atom/ion beam. Only a cursory description of the experimental method is given here, since the apparatus and technique have been described in many previous publications on other species. The reader is referred to recent work in Eu I, II, and III (Den Hartog et al. 2002) for a more detailed description.

A slow ($\sim 5 \times 10^4$ cm/s), weakly collimated beam of Gd atoms and ions is produced using a hollow cathode discharge sputter source. A pulsed argon discharge, operating at ~ 0.4 torr with 10 μ s duration, 10 A pulses, is used to sputter the gadolinium which lines the hollow cathode. The hollow cathode is closed on one end except for a 1 mm hole, through which the gadolinium atoms and ions flow into a low pressure (10^{-4} torr) scattering chamber. This beam is intersected at right angles by a nitrogen laser-pumped dye laser beam 1 cm below the cathode bottom. The laser is tunable over the range 2050 - 7200 Å with the use of frequency doubling crystals, is pulsed at ~ 30 Hz repetition rate with a ~ 3 ns pulse duration, and has a ~ 0.2 cm $^{-1}$ bandwidth. The laser is used to selectively excite the level to be studied, eliminating the possibility of cascade radiation from higher-lying levels.

Fluorescence is collected at right angles to the laser and atomic/ionic beams through a pair of fused-silica lenses which form an f/1 optical system, and detected with a RCA 1P28A photomultiplier tube (PMT). Optical filters, either broadband colored glass filters or narrowband multi-layer dielectric filters, are typically inserted between the two lenses to cut down on scattered laser light and to block cascade radiation from lower levels. The signal from the PMT is recorded and averaged over 640 shots using a Tektronix SCD1000 digitizer. Data collection begins after the laser pulse has terminated to make deconvolution of the laser excitation unnecessary. Data are recorded with the laser tuned on and off the excitation transition. A linear least-square fit to a single exponential is performed on the background-subtracted fluorescence decay to yield the lifetime of the level. The lifetime is measured twice for each level, using a different excitation transition whenever possible. This redundancy helps ensure that the transitions are identified correctly in the experiment, classified correctly and are free from blends.

The lifetimes reported here have an uncertainty of $\pm 5\%$, except for the shortest lifetimes (< 4 ns) for which the uncertainties are ± 0.2 ns. To achieve this level of fidelity and maintain it over the full dynamic range of the experiment (2 ns to 1.5 μ s for ions), the possible systematic errors in these measurements must be well understood and controlled. They include electronic bandwidth limitations, cascade fluorescence, Zeeman quantum beats and atomic motion flight-out-of-view effects, among others. The dominant systematic error depends on the lifetime, for example the bandwidth, linearity, and overall fidelity of

the electronic detection system prevents us from achieving better than ± 0.2 ns accuracy even on short lifetimes. These systematic effects are discussed in detail in earlier publications, (See, for example, Den Hartog et al. 1999; 2002) and will not be discussed further here. As a means of verifying that the measurements are within the stated uncertainties, we perform periodic end-to-end tests of the experiment by measuring a set of well known lifetimes. These cross-checks include lifetimes of Be I (Weiss 1995), Be II (Yan et al. 1998) and Fe II (Guo et al. 1992; Biémont et al. 1991), covering the range from 1.8–8.8 ns. An Ar I lifetime is measured at 27.85 ns (Volz & Schmoranzner 1998). He I lifetimes are measured in the range 95 – 220 ns (Kono & Hattori 1984).

The results of our lifetime measurements of 49 even-parity and 14 odd-parity levels of Gd II are presented in Table 1. Energy levels are from the tabulation by Martin et al. (1978). Air wavelengths are calculated from the energy levels using the standard index of air (Edlén 1953). The uncertainty of the lifetimes is the larger of $\pm 5\%$ or ± 0.2 ns.

Also presented in Table 1 is a comparison of our results with those from other LIF lifetime measurements available in the literature. We see very good agreement with the recent work of Xu et al. (2003). They measured lifetimes for 13 even-parity levels of Gd II, of which 11 were in common with our study. All of our measurements agreed within our joint error bars except for the level at 29198 cm^{-1} , which was only slightly worse than that. We found a mean difference between our measurements and theirs of 0.0% and a rms difference of 5.6%. Our measurements also agree very well with those of Zhang et al. (2001a). They measured lifetimes for 20 even-parity levels of Gd II, all of which overlap with our study. All of the lifetimes agreed within the joint uncertainties and we see a -0.4% mean difference and 6.8% rms difference between our measurements and theirs. The comparison to the three lifetimes measured by Bergström et al. (1988) is less satisfactory, particularly for the level 30009 cm^{-1} , for which their result is considerably lower than our measurement and that of Zhang et al.. The mean and rms differences between our measurements are -15.8% and 17.9%, respectively, for these three levels.

Two older sets of measurements exist giving lifetimes of a total of six levels of Gd II, using the delayed-coincidence method with non-selective electron beam excitation. Gorshkov et al. (1983) report lifetimes on four levels and Gorshkov & Komarovskii (1986) on two additional. These lifetimes are all substantially longer than ours and other LIF results (by as much as a factor of 3), probably due to cascade from higher-lying levels because of the non-selective nature of the electron beam excitation. These results are not included in Table 1.

3. BRANCHING FRACTIONS AND ATOMIC TRANSITION PROBABILITIES

Branching fraction measurements in complex RE spectra such as Gd II require an extremely powerful spectrometer. As in earlier work on RE spectra, we used the 1.0 meter FTS at the National Solar Observatory (NSO) for this project. This instrument has the large etendue of all interferometric spectrometers, a limit of resolution as small as 0.01 cm^{-1} , wavenumber accuracy to 1 part

in 10^8 , broad spectral coverage from the UV to IR, and the capability of recording a million point spectrum in 10 minutes (Brault 1976). An FTS is insensitive to any small drift in source intensity since an interferogram is a simultaneous measurement of all spectral lines.

Figure 1 is a partial Grotrian diagram for Gd II. Although there are nine valence electrons in singly ionized Gd, seven of the nine form a half completed 4f shell. The high spin of the half completed 4f shell leads to rich, but not overwhelmingly complex, energy level structure. Low odd- and even-parity configurations are built by putting the remaining two valence electrons into some combination of 5d, 6s, 4f, and/or 6p orbitals. Most of the low odd- and even-parity levels have sufficiently pure LS coupling, that they can be assigned using that coupling scheme. Energy ranges of important low-lying odd- and even-parity levels of each sub-configuration are marked in Fig. 1, as well as the energy ranges and sub-configurations of the upper levels studied in this work.

The nine valence electrons of singly ionized Gd yield low odd-parity levels, including the ground level, in the $4f^7(^8S)(5d+6s)^2$ sub-configurations. The tight coupling of the 4f electrons to form the 8S parent term is not broken until about $32,500 \text{ cm}^{-1}$ (Cowan 1981, Blaise et al. 1971). All 20 levels of the $^{10}D^o$, $^8D^o$, $^8D^o$, and $^6D^o$ terms of the $4f^7(^8S)5d6s$ sub-configuration are known, as is the $4f^7(^8S)6s^2^8S^o$ level. The $4f^7(^8S)5d^2$ sub-configuration contains 43 levels in the $^8G^o$, $^{10}F^o$, $^8F^o$, $^6F^o$, $^8D^o$, $^{10}P^o$, $^8P^o$, $^6P^o$, and $^8S^o$ terms, all of which are also known. These low odd-parity levels are spread from the ground $4f^7(^8S)5d(^9D)6s \ ^{10}D_{5/2}^o$ level at 0.00 cm^{-1} to the $4f^7(^8S)5d^2(^1S) \ ^8S_{7/2}^o$ level at $\sim 29,000 \text{ cm}^{-1}$. The next band of observed odd-parity levels are part of the $4f^8(^7F)6p$ sub-configuration that starts at $\sim 33,000 \text{ cm}^{-1}$ (see Table IX of Blaise et al. 1971 for predictions of unobserved $4f^8 6p$ levels).

The low even-parity levels start just under 8000 cm^{-1} with 13 levels of the 8F and 6F terms of the $4f^8(^7F)6s$ sub-configuration. The 57 levels of the 8H , 6H , 8G , 6G , 8F , 6F , 8D , 6D , 8P , and 6P terms of the $4f^8(^7F)5d$ sub-configuration are all known. These levels start $\sim 18,000 \text{ cm}^{-1}$ and extend to $\sim 32,000 \text{ cm}^{-1}$. Although the $4f^7(^8S)(6s+5d)6p$ sub-configuration starts around $26,000 \text{ cm}^{-1}$, it appears that all even-parity levels in the $25,000 \text{ cm}^{-1}$ to $30,000 \text{ cm}^{-1}$ range have been observed (see Fig. 1 of Blaise et al. 1971). Two perturbed levels assigned to the $4f^8(^5D)6s$ sub-configuration have been found at 26352 cm^{-1} and 27274 cm^{-1} (Blaise et al. 1971). The absence of low-lying unobserved levels simplified the assessment of missing branches or residuals in our branching fraction measurements and provided high confidence in a partition function evaluation. The interleaving of low even- and odd-parity levels made it possible for us to measure lifetimes and transition probabilities for upper levels of both parities.

The upper levels studied in this work have significant 6p character as indicated in Table 1. The odd-parity upper levels are part of the $4f^8(^7F)6p$ sub-configuration. The even-parity upper levels are from the $4f^7(^8S)6s6p$ and $4f^7(^8S)5d6p$ sub-configurations. Energy ranges of the upper levels are indicated in Fig. 1.

In order to make our branching fraction measurements as complete as possible, we worked on the 16 spectra listed in Table 2. We recorded some of these spectra during observing runs in the 2000 through 2002 period and extracted the older spectra from the NSO electronic archives¹. The former spectra are of commercially manufactured, sealed Gd hollow cathode discharge (HCD) lamps with fused silica windows containing either argon or neon buffer gas fills. Although these small lamps typically yield spectra with minimal optical depth or radiation trapping effects, we still recorded a few spectra at reduced currents to check for such effects. Our most useful spectra were recorded using the small lamps at 20 to 30 mA currents with many, ~ 50 , coadds. These small commercial lamps were designed for atomic absorption spectrophotometers used by analytical chemists, and they are usually very stable which is crucial for recording good interferograms. (Lamp oscillations can easily wreck an interferogram by introducing spurious modulations that result in ghosts in the final spectrum.) The 20 to 30 mA currents are above the manufacturer’s recommended maximum current. We used forced air cooling during all-night integrations to get our most useful spectra. This approach shortens the lamp lifetimes, but yields the most valuable, optically thin spectra with good S/N ratios covering wide spectral regions. The custom (water cooled) HCD lamp and electrodeless discharge lamp (EDL) yielded spectra with superior S/N ratios for many weak lines with branching fractions as small as 0.001. The high currents (> 100 mA) in the custom HCD resulted in some optical depth effects on the strongest Gd II lines to low odd-parity levels. These potential errors were identified and eliminated by comparing the high- and low-current HCD spectra. The comparison of spectra with Ne and Ar buffer gas was used to eliminate potential errors from blends of buffer gas lines with lines of Gd II.

The establishment of an accurate relative radiometric calibration or efficiency is critical to a branching fraction experiment. As indicated in Table 2, we made greater use of standard lamp calibrations in this Gd II study than in previous RE studies. We are constantly trying to improve our radiometric calibrations of the FTS, because such calibrations are thought to be the dominant source of uncertainty for many of our final $\log(gf)$ values. Tungsten (W) filament standard lamps are particularly useful near the Si detector cutoff in the 10,000 to 9,000 cm^{-1} range where the FTS sensitivity is changing rapidly as a function of wave number, and near the dip in sensitivity at 12,500 cm^{-1} from the aluminum coated optics. Tungsten lamps are not bright enough to be useful for FTS calibrations in the UV region, and UV branches typically dominate the decay of levels studied using our lifetime experiment. In general one must be careful when using continuum lamps to calibrate the FTS over wide spectral ranges, because the “ghost” of a continuum is a continuum. The Ar I and Ar II line technique, which is internal to the HCD Gd/Ar lamp spectra, is still our preferred calibration technique. It captures the wavelength-dependent response of detectors, spectrometer optics, lamp windows, and any other components in the light path or any reflections which contribute to the detected signal (such

¹The NSO archives are available at <http://nsokp.nso.edu/dataarch.html>

as due to light reflecting off the back of the hollow cathode). This calibration technique is based on a comparison of well-known branching ratios for sets of Ar I and Ar II lines widely separated in wavelength, to the intensities measured for the same lines. Sets of Ar I and Ar II lines have been established for this purpose in the range of 4300 to 35000 cm^{-1} by Adams & Whaling (1981), Danzmann & Kock (1982), Hashiguchi & Hasikuni (1985), and Whaling et al. (1993). One of our best Gd/Ar HCD spectra from 2002, and some the Gd/Ar HCD spectra from 1991, can also be calibrated with tungsten standard lamp spectra recorded shortly before, or after, the HCD lamp spectra. The older tungsten lamp is a strip lamp calibrated as a spectral radiance ($\text{W}/(\text{m}^2 \text{ sr nm})$) standard, and the newer is a tungsten-quartz-halogen lamp calibrated as a spectral irradiance ($\text{W}/(\text{m}^2 \text{ nm})$ at a specified distance) standard. Neither of these filament lamps is hot or bright enough to yield a reliable UV calibration, but they are useful in the visible and near IR for interpolation and as a redundant calibration. Argon calibration lines were largely absent in the EDL spectra, and thus these spectra were calibrated using the tungsten lamps.

All possible transition wave numbers between known energy levels of Gd II satisfying both the parity change and $\Delta J = -1, 0, \text{ or } 1$ selection rules were computed and used during analysis of FTS data. Energy levels from Martin et al. (1978) were used to determine possible transition wave numbers. Levels from Martin et al. (1978) are available in electronic form from Martin et al. (2000)².

Branching fraction measurements were attempted on lines from all 63 levels of the lifetime experiment, and were completed for lines from 39 even-parity and 13 odd-parity upper levels. The levels for which branching fractions could not be completed had a strong branch beyond the UV limit of our spectra, or had a strong branch which was severely blended. Typically an upper level, depending on its J value, has about 30 possible transitions to known lower levels. More than 20,000 possible spectral line observations were studied during the analysis of 16 different Gd/Ar and Gd/Ne spectra. We set baselines and integration limits “interactively” during analysis of the FTS spectra. The same numerical integration routine was used to determine the un-calibrated intensities of Gd II lines and selected Ar I and Ar II lines used to establish a relative radiometric calibration of the spectra. A simple numerical integration technique was used in this and most of our other RE studies because of weakly resolved or unresolved hyperfine and isotopic structure. More sophisticated profile fitting is used only when the line sub-component structure is either fully resolved in the FTS data or known from independent measurements.

The procedure for determining branching fraction uncertainties was described in detail by Wickliffe et al. (2000). Branching fractions from a given upper level are defined to sum to unity, thus a dominant line from an upper level has small branching fraction uncertainty almost by definition. Branching fractions for weaker lines near the dominant line(s) tend to have uncertainties limited by their S/N ratios. Systematic uncertainties in the radiometric calibration are

²Available at http://physics.nist.gov/cgi-bin/AtData/main_asd

typically the most serious source of uncertainty for widely separated lines from a common upper level. We used a formula for estimating this systematic uncertainty that was presented and tested extensively by Wickliffe et al. (2000). The spectra of the high current HCD lamp and EDL's enabled us to connect the stronger visible and near IR branches to quite weak branches in the same spectral range. Uncertainties grew to some extent from piecing together branching ratios from so many spectra, but such effects have been included in the uncertainties on branching fractions of the weak visible and near IR lines. In the final analysis, the branching fraction uncertainties are primarily systematic. Redundant measurements with independent radiometric calibrations help in the assessment of systematic uncertainties. Redundant measurements from spectra with different discharge conditions also make it easier to spot blended lines and optically thick lines.

Branching fractions from the FTS spectra were combined with the radiative lifetime measurements described in §2 to determine absolute transition probabilities for 611 lines of Gd II in Table 3. Air wavelengths in Table 3 were computed from energy levels (Martin et al. 1978) using the standard index of air (Edlén 1953). Parities are included in Table 3 using the “ev” and “od” notation introduced in Table 1.

Transition probabilities for the very weakest lines (branching fractions < 0.001) which were observed with poor S/N ratios and for a few blended lines are not included in Table 3, however these lines are included in the branching fraction normalization. The effect of the problem lines becomes apparent if one sums all transition probabilities in Table 3 from a chosen upper level, and compares the sum to the inverse of the upper level lifetime from Table 1. Typically the sum of the Table 3 transition probabilities is between 95% and 100 % of the inverse lifetime. Although there is significant fractional uncertainty in the branching fractions for these problem lines, this does not have much effect on the uncertainty of the stronger lines that were kept in Table 3. Branching fraction uncertainties are combined in quadrature with lifetime uncertainties to determine the transition probability uncertainties in Table 3. Possible systematic errors from missing branches to unknown lower levels are negligible in Table 3, because we were able to make at least rough measurements on visible and near IR lines with branching fractions as small as 0.001. The radiative lifetimes of the Gd II levels in this study are generally shorter than the radiative lifetimes we studied in Sm II (LDSC06). The generally short Gd II lifetimes, in combination with the frequency cubed scaling of transition probabilities, means that any unknown line in the mid- to far-IR region will not have a significant branching fraction.

We have searched the literature unsuccessfully for any recent branching fraction measurements or calculations on Gd II. The only published branching fraction or transition probability measurements we found are based on photographic data from the National Bureau of Standards. Relative intensity measurements by Meggers et al. (1961) were converted to absolute transition probabilities by Corliss & Bozman (1962). Ward (1985) reported a formula for re-normalizing the Corliss & Bozman (1962) transition probabilities. Cowley & Corliss (1983)

developed a formula for determining transition probabilities from line intensities published by Meggers et al. (1975) which are an updated version of the original Meggers et al. (1961) line intensities used by Corliss & Bozman (1962). The problems with the 1961 data set are illustrated by efforts to renormalize it, and they have been discussed extensively (e.g. Obbarius & Kock 1982).

4. SOLAR AND STELLAR GADOLINIUM ABUNDANCES

We have employed the new Gd II transition probabilities to re-determine gadolinium abundances for the solar photosphere and three very metal-poor ($[\text{Fe}/\text{H}] < -2$)³ stars that have large overabundances of the rare-earth elements. These are stars enriched in rapid n -capture (r -process) nucleosynthesis products: HD 115444 ($[\text{Fe}/\text{H}] = -2.9$, $[\text{Eu}/\text{Fe}] = +0.8$, Westin et al. 2000); BD+17°3248 ($[\text{Fe}/\text{H}] = -2.1$, $[\text{Eu}/\text{Fe}] = +0.9$, Cowan et al. 2002), and CS 22892-052 ($[\text{Fe}/\text{H}] = -3.1$, $[\text{Eu}/\text{Fe}] = +1.5$, Sneden et al. 2003). Our abundance study followed the methods used in previous papers of this series, most closely resembling those employed for Sm II by LDSC06.

4.1 Line Selection

We have accurate transition probabilities for 611 Gd II lines, but not all of these lines are useful in Gd abundance analyses. For our program objects, the majority of the Gd II lines prove to be either undetectably weak, or heavily blended with other species transitions, or both. Here we describe the Gd II line selection procedures. As discussed by LDSC06, in a standard LTE abundance analysis the relative strengths of lines of an individual species vary directly as the transition probabilities modified by the Boltzmann excitation factors. Thus for a weak line on the linear part of the curve-of-growth the equivalent width (EW) and reduced width (RW) are related as, $\log(\text{RW}) \equiv \log(\text{EW}/\lambda) \propto \log(gf) - \theta\chi$, where excitation energy χ is in units of eV and inverse temperature $\theta \equiv 5040/\text{T}$. The relative strengths of lines of different species also depend on relative elemental abundances and Saha ionization equilibrium factors. However, Gd and Sm have similar low ionization potentials, 6.150 eV and 5.644 eV, respectively (Grigoriev & Melikhov 1997). (All RE's have first ionization potentials within 0.5 eV of 5.9 eV.) In line-forming atmospheric layers ($\tau \geq 0.1$) of the Sun and stars considered here, Gd and Sm exist almost exclusively in their ionized states: $n_{II}/n_I > 100$, or $n_{II} \approx n_{total}$. Therefore, for the ionized-species transitions studied by LDSC06 and here, the Saha corrections to account for other ionization state populations are negligible. In this case the relative strength factors of weak lines can be written as $\text{STR} \equiv \log(\varepsilon gf) - \theta\chi$, where ε is the elemental abundance.

In Figure 2 we plot these relative strength factors as a function of wavelength for Sm II (LDSC06) and Gd II lines. To compute these strength factors we have

³We adopt standard stellar spectroscopic notations that for elements A and B, $[\text{A}/\text{B}] = \log_{10}(\text{N}_A/\text{N}_B)_{star} - \log_{10}(\text{N}_A/\text{N}_B)_{sun}$, for abundances relative to solar, and $\log \varepsilon(\text{A}) = \log_{10}(\text{N}_A/\text{N}_H) + 12.0$, for absolute abundances.

adopted solar abundances of $\log \varepsilon(\text{Sm}) = +1.00$ (LDSC06), and $\log \varepsilon(\text{Gd}) = +1.10$ (close to the recommended photospheric abundance of Grevesse & Sauval 2002, Lodders 2003, and the new value derived in this paper).

In Figure 2 we have indicated the approximate minimum strength factor for lines at the detection threshold in the solar spectrum. This limiting strength case has been computed as follows. LDSC06 searched the very high-resolution, high S/N solar center-of-disk spectrum of Delbouille et al. (1973) for the weakest solar Sm II lines that could be reliably detected and employed in an abundance analysis. That exercise suggested a lower limit for unblended lines of $\text{EW} \approx 1.5$ mÅ in the blue spectral region ($\lambda \sim 4500$ Å), or $\log(\text{RW}) \approx -6.5$. Lines of Sm II near this limit had values of $\log(gf) - \theta\chi \approx -1.6$, which translates to $\text{STR} \approx -0.6$. The equivalent width detection limit should also apply to Gd II, and so that limit has been indicated in both panels of the figure with horizontal dotted lines.

In Figure 2 we also show the minimum strength factor for Sm II and Gd II lines that exhibit substantial absorption in the solar spectrum. This is a fairly arbitrary assignment. Beginning at the defined detection-limit $\text{STR} = -0.6$, a line 20 times stronger will have $\text{STR} = -0.6 + 1.3 = +0.7$. If such lines remained on the linear (unsaturated) part of the curve-of-growth then the increase in equivalent width would be identical: $\log(\text{RW}) = -6.5 + 1.3 = -5.2$, or $\text{EW} \approx 30$ mÅ near 4500 Å. In reality lines in this RW regime are slightly saturated; test calculations suggest that the solar Sm II and Gd II lines with strength factors 20 times larger than the detection limit will have $\log(\text{RW}) \approx -5.35$, or $\text{EW} \approx 20$ mÅ at 4500 Å. We adopt $\text{STR} = +0.7$ as the lower limit for strong lines in this study, and have drawn dashed horizontal lines to indicate this in the figure.

Inspection of Figure 2 reveals similarities and differences in the transitions of Sm II and Gd II. First, essentially all useful lines for a solar abundance analysis have wavelengths $\lambda < 5000$ Å. This is especially true for Gd II, for which nearly all lines above the defined detection threshold occur at $\lambda < 4500$ Å. Second, Gd II has many more strong lines (more than 40 with $\text{STR} > +0.7$) potentially available for abundance analysis than did Sm II (only 4). However, all strong lines of both species are located in the near-UV, $\lambda < 4000$ Å, where the line density is large. None of these lines are unblended, so that attempts to derive abundances from an equivalent width analysis are risky. For Gd II especially, the lack of many potentially detectable lines in the less crowded spectral regions redward of 4500 Å emphasizes the necessity of computing full synthetic spectra for all transitions used in the final analysis.

As in LDSC06, the strength factor plot of Figure 2 was used to make the first cut in reducing the original large list of Gd II lines to a more manageable list for the solar/stellar work. Of the 611 lines with laboratory transition probabilities newly determined in this paper, 235 have $\text{STR} \geq -0.6$. Attempts to detect useful transitions among the 376 Gd II lines below this strength level in the solar spectrum failed with one exception (see below). These weaker lines were therefore discarded.

We then followed the procedures described in LDSC06 and earlier papers of

this series to identify the final set of Gd II lines to be used in the solar/stellar abundance analyses. With the aid of the Delbouille et al. (1973) solar center-of-disk spectrum, the Moore, Minnaert, & Houtgast (1966) solar line identification atlas, the Kurucz (1998) atomic and molecular line compendium, and the observed spectrum of the r -process-rich metal-poor giant star BD+17° 3248 (Cowan et al. 2002), we eliminated about 150 more Gd II lines that proved to be undetectably weak, extremely blended, or both. Some examples of this elimination process are discussed by LDSC06. All of the preliminary culling efforts finally produced a list of about 80 lines worthy of closer inspection in solar and/or stellar spectra.

4.2 The Solar Photospheric Gadolinium Abundance

We employed synthetic spectrum computations to determine a new gadolinium abundance for the solar photosphere. The procedures were identical to those described by LDSC06. We employed Kurucz’s (1998) line database and Moore et al.’s (1966) solar identifications to generate lists of relevant atomic and molecular lines in 4-6 Å regions surrounding each Gd II transition. We used (a) these line lists, (b) the Holweger & Müller (1974) solar model atmosphere, and (c) a standard solar abundance set drawn from reviews by Grevesse & Sauval (1998, 2002) and Lodders (2003) supplemented by values determined in earlier papers of this series, as inputs into the current version of the LTE line analysis code MOOG (Snedden 1973) to generate the synthetic spectra. We adopted some well-determined transition probabilities for ionized species of neutron-capture elements from the following sources: Gd, the present work; La, Lawler et al. (2001a); Nd, Den Hartog et al. (2003); Eu, Lawler et al. (2001b); Sm, LDSC06, Tb, Lawler et al. (2001c); Dy, Wickliffe et al. (2000); Ho, Lawler et al. (2004); Ce, Palmeri et al. (2000); Y, Hannaford et al. (1982); and Zr, Malcheva et al. (2006).

We computed multiple synthetic spectra for each Gd line region, and compared them to the Delbouille et al. (1973) center-of-disk photospheric spectrum. We smoothed the spectra empirically by a Gaussian to match the observed line broadening due to solar macroturbulence and spectrograph instrumental effects. The oscillator strengths for contaminant atomic transitions (except for the species listed above) were adjusted to fit the solar spectrum. Molecular line strengths were altered as a group via abundance changes of C, N, or O as appropriate. For unidentified solar features, we arbitrarily added Fe I lines with excitation potentials $\chi = 3.5$ eV to the line lists. The initial synthetic spectrum computations showed that the majority of the proposed Gd II transitions are very blended or very weak in the solar spectrum, thus useless in a Gd photospheric abundance analysis. The iterated line lists for these discarded solar Gd II features were retained for further investigation in the r -process-rich stellar spectra (§ 4.3).

In the end we used just 20 carefully selected Gd II lines in the solar spectrum. In the left-hand panels (a), (b), and (c) of Figure 3 we show synthetic and observed spectra of three representative transitions. Panel (a) contains two

neighboring Gd II lines that are commonly employed in studies of r -process-rich metal-poor stars because they are relatively strong and located in the commonly observed spectral region near 4000 Å. Panel (b) shows a relatively strong line (STR $\approx +1.1$) that suffers only modest contamination from other species in spite of its location at 3549 Å. Finally, panel (c) demonstrates that one of the strongest Gd II lines (STR $\approx +1.3$) can be detected with confidence even though its wavelength of 3358 Å lies in the middle of a strong band of NH.

The derived abundances for individual Gd II lines are listed in column 4 of Table 4, and are displayed as a function of wavelength in Figure 4. A straight mean abundance is $\log \varepsilon(\text{Gd}) = 1.11 \pm 0.01$ ($\sigma = 0.05$, 20 lines). The abundances show no obvious trend with wavelength (Figure 4), excitation potential (although the range is small), $\log(gf)$, or general line strength.

The two lines at the wavelength extremes of our solar list deserve comment. Moore et al. (1966) identifies a solar absorption at 5733.89 Å as Gd II, with EW = 1 mÅ, or $\log(\text{RW}) = -6.8$. This is the weakest line that they attribute to Gd II, and is 0.3 dex smaller than our suggested weak-line limit. The absorption at this wavelength appears also in the Delbouille et al. (1973) photospheric spectrum, so we included it in our analysis, deriving $\log \varepsilon = 1.15$, consistent with the mean abundance. We were unable to identify any other solar Gd lines in this strength regime. Moore et al. also identify a strong line at 3032.84 Å as Gd II. Because this line is in the very crowded near-UV spectral region and their identifications were from relatively noisy photographic spectra, Moore et al. did not estimate an equivalent width for this line. Our analysis confirms its identification, and the derived abundance of $\log \varepsilon = 1.10$ is in excellent accord with the mean. The 3032 Å line is the shortest-wavelength solar feature that we have been able to model successfully in this series of papers.

Abundance uncertainties can be due to line profile matching factors (internal uncertainties) and scale factors (external uncertainties). For the present Gd analysis these issues are nearly identical to those outlined for Sm by LDSC06. Transition profile fitting uncertainties are estimated at ± 0.02 dex, and on average the uncertainties due to contamination by other species lines are also ± 0.02 dex. The mean error in $\log(gf)$ for the 20 lines used in the solar analysis (see Table 4) is ± 0.03 . Adding these uncertainties in quadrature yields an estimated total internal uncertainty of ± 0.04 dex, which is close to the observed $\sigma = 0.05$.

Overall scale errors can arise from other atomic data uncertainties and model atmosphere choices. As stated in §4.1, Saha-fraction corrections are negligible for Gd II, so the derived Gd abundance depends directly on the Boltzmann factor and the Gd II partition function. We checked Irwin’s (1981) polynomial representation of the temperature dependent Gd II partition function against a partition function evaluated from the online NIST energy levels (Martin et al. 2000). We found nearly perfect agreement, as expected, because the lower levels of Gd II which determine the partition function for $T < 6000$ K are all known.

The influence of solar model atmosphere choice was assessed by repeating sample abundance derivations using the Kurucz (1998) and Grevesse & Sauval (1999) models, finding on average abundance shifts of -0.01 and -0.02 dex, respectively, with respect to those derived with the Holweger & Müller (1974)

model. These differences are nearly identical to those determined for other rare earth ions in the previous papers of this series. Therefore abundance scale errors appear to be very small, of order 0.02 dex, within the limits imposed by our analysis assumptions (single-stream, plane-parallel atmosphere geometry, LTE). Combining internal line-to-line scatter uncertainties (which contribute just ± 0.01 in the mean abundance, since 20 lines are employed here) and external scale uncertainties, we recommend $\log \varepsilon(\text{Gd})_{Sun} = +1.11 \pm 0.03$.

This new Gd abundance is in agreement with the result of the only other solar photospheric analysis in the past two decades. From an equivalent width analysis of eight lines, Bergström et al. (1988) derived $\log \varepsilon(\text{Gd})_{Sun} = +1.12 \pm 0.04$, where their uncertainty estimate was set to twice the standard deviation of the mean abundance. Note that seven of their chosen eight lines have also been included in our study. The photospheric abundance appears to be slightly higher than the recommended meteoritic abundances in two recent compilations: $\log \varepsilon(\text{Gd})_{met} = +1.06 \pm 0.02$ (Lodders 2003), and $+1.03 \pm 0.02$ (Asplund, Grevesse, & Sauval 2005). This point will be considered again in §5.

4.3 Gadolinium Abundances in Three r -Process-Rich Low Metallicity Stars

We next explored the Gd II spectra of very metal-poor, r -process-rich giant stars BD+17°3248, HD 115444, and CS 22892-052. Spectra of such stars present much more favorable cases for the study of Gd II and other rare-earth first ions. This is due to the confluence of several effects: overall metal deficiency; relative n -capture-element enhancement; and lower stellar temperatures and gravities than the Sun (which combine to weaken the numerous high excitation neutral-species transitions and strengthen low excitation ionized-species ones). Many Gd II lines that are too blended and/or weak in the solar spectrum can be analyzed reliably in the r -process-rich stars. We illustrate this in right-hand panels (d), (e), and (f) of Figure 3, displaying the same Gd II lines that were previously shown in the solar spectrum. The central depths of the Gd lines are similar in the Sun and BD+17°3248. However, the total absorptions and thus equivalent widths are larger in BD+17°3248 because the line breadths are larger in the star (this is mainly an effect of the coarser resolution of this and the other two stellar spectra). Although the Gd II lines are typically stronger in the r -process-rich stars than in the Sun, the lower resolution and S/N of the stellar spectra changed the detection-with-confidence limit to about 3 mÅ near 4500 Å, about double that of the solar spectrum. Therefore the strength factor detection limit was roughly the same in solar and stellar cases, and we made no attempt to re-visit the entire Gd line list to discover additional very weak Gd II lines.

We derived Gd abundances for the stars in the same manner as was described for the Sun in § 4.2. The abundances from individual lines are listed in Table 4 and displayed in Figure 4. The mean abundances, standard deviations, and number of lines are given at the bottom of Table 4 and Figure 4. The line-to-line

scatters are all small, $\sigma = 0.04 - 0.07$, and are mainly due to stellar spectrum measurement uncertainties.

5. ABUNDANCES OF n -CAPTURE ELEMENTS IN METAL-POOR HALO STARS

The new laboratory atomic data, particularly transition probabilities, are critical to

abundance determinations of the n -capture elements in the metal-poor (old) Galactic halo stars. These ongoing abundance studies are providing new information about the nature of the earliest Galactic nucleosynthesis and the nature of the earliest stars - those that preceded the formation of the halo stars (Cowan & Sneden 2006). Increasingly more accurate stellar abundances have also recently allowed detailed comparisons with solar system distributions (Den Hartog et al. 2003; Lawler et al. 2004, 2006). Such abundance comparisons are providing new and more complete understandings of the nuclear processes and the astrophysical sites for heavy element nucleosynthesis.

In Figure 5 we illustrate the n -capture abundances in the atomic number range $56 \leq Z \leq 68$ for the Solar System and for the three very metal-poor ($[\text{Fe}/\text{H}] < -2$) halo giant stars CS 22892-052, HD 115444 and BD+17° 3248. We have plotted the abundance differences (log observed abundance *minus* log solar system r -process only value) for each element in each star. For this comparison we have normalized the abundance distributions of all three stars at the r -process element Eu. The solar system elemental

r -process abundance distribution was obtained by summing the individual r -process isotopic abundance contributions, based upon the so-called standard model (see Simmerer et al. 2004; Cowan et al. 2006 and the discussion below).

If the stellar and solar r -process abundance values were identical they would fall on the solid horizontal line in the figure - i.e., $\log \varepsilon(\text{X})_{\text{obs}} - \log \varepsilon(\text{X})_{\text{s.s.}(r\text{-only})} = 0$. Abundance comparisons between the stellar elemental abundances for Gd and other n -capture elements with the total Solar System meteoritic abundance values (dotted-line curve) from Lodders (2003) are also shown. We show the abundances in the top panel of this figure from the original published papers by our group (Westin et al. 2000; Cowan et al. 2002; Sneden et al. 2003). It is clear that there was a large amount of scatter for a number of elements including Nd, Sm, Ho and Gd in the stellar data. Reducing or eliminating this abundance scatter has been one of the prime motivations to obtain improved laboratory data for various elements of astrophysical interest.

In the bottom panel of Figure 5 we show the newly revised abundances, utilizing the new transition probabilities for the elements Nd (Den Hartog et al. 2003), Ho (Lawler et al. 2004), Sm (LDSC06) and Gd from this paper. As a result of employing these new atomic data, the star-to-star scatter is greatly reduced, and there is good agreement between the elemental values in CS 22892-052, HD 115444 and BD+17° 3248 and the solar system r -process values. This good agreement is further support for the finding that the abundances of the stable elements (at least for Ba and above) are consistent with the scaled solar

system elemental r -process distribution. (see, *e.g.*, Truran et al. 2002; Sneden & Cowan 2003 and Cowan & Sneden 2006). It also again demonstrates that early in the history of the Galaxy the r -process was the dominant synthesis mechanism, as the n -capture elements seen in these stars were formed in the r -process only, and not the s -process. Many of the rare earth elements have a significant s -process component in solar system material (*e.g.*, Nd is 58% s -process and Sm is 33% s -process, Simmerer et al. 2004) – this can be seen in Figure 5 as the differences between the total solar photospheric abundances (black dots with dotted line from Lodders 2003) and the stellar (r -process) elemental abundances. However, since the predominant s -process synthesis is coming from low-mass long-lived stars (Busso et al. 1999), there is not sufficient time early in the history of the Galaxy for these stars to live, die and eject s -process enriched material into the ISM prior to the formation of the observed halo stars. Instead, all of these elements must have been synthesized in relatively high-mass, rapidly-evolving stars that presumably exploded as core-collapse supernovae and enriched the gas in the early Galaxy (Cowan & Thielemann 2004; Cowan & Sneden 2006).

5.1 Solar and Stellar Abundance Comparisons

The detailed solar and stellar abundance comparisons depend upon the deconvolution of Solar System material into separate isotopic s - and r -process contributions. The individual s -process isotopic abundances are first determined

(often) employing the so called “classical model” approximation in conjunction with measured neutron capture cross-sections. A more complicated “stellar model” approach to obtaining the s -process contributions has also been made (Arlandini et al. 1999).

Cross-section measurements are not possible for the far more radioactive and short-lived r -process nuclei. The r -process isotopic abundances (or residuals) are therefore determined by just subtracting the calculated s -process abundances from the total Solar System abundances. We have tabulated in Cowan et al. (2006) the individual s - and r -process isotopic solar system abundances (based upon the $\text{Si} = 10^6$ scale and assuming the classical model approximation) from the work of Käppeler et al. (1989), Wisshak et al.(1998) and O’Brien et al. (2003). The solar system r -process (only) elemental abundance curve, such as the one employed in Figure 5 (and labeled as $\log \varepsilon(X)_{S.S.(r\text{-only})}$), is obtained by summing the individual isotopic contributions from the r -process. (Similarly, the s -process only elemental abundance curve is the sum of the s -process contributions.)

In spite of Figure 5’s very good overall agreement between the abundances of the rare-earth elements in the halo stars and the solar system r -process abundances discussed above, some small deviations have become more apparent as RE transition probabilities have improved. For example, in the bottom panel of Figure 5 the Gd abundances in the three halo stars are clustered together

slightly above the (meteoritic-based) Solar System r -process (only) value – implying that the solar system abundance might be too low.

The increasingly accurate stellar abundances could possibly be used to predict specific r -process abundances directly, rather than obtaining the residuals in the manner described above. We have attempted to do this, based upon the following procedure. First, we list in Table 5 the s -process (N_s) and r -process (N_r) contributions to a RE element. Those abundances (based upon the Si = 10^6 scale and assuming the classical model approximation) are listed in Table 5 (see also Cowan et al. 2006 for a complete list). Next we determined the difference between $\log(N_r(\text{el})) - \log(N_r(\text{Eu}))$ for each element. That result was compared with the average difference between the RE elements and Eu (almost entirely an r -process element), $\langle \text{el-Eu} \rangle$, for the three halo stars. Assuming that this average value was the correct one, we obtained a predicted solar system r -process abundance, $N_r(\text{predicted})$ – this would be the value that would raise the solid line to be coincident with the stellar data. Thus, in the case of Gd, we obtain a value of $N_r(\text{predicted}) = 0.312$, rather than the previously determined value of 0.276. This implies that the solar r -process only value for Gd should be raised by that difference. Finally, assuming that the previously predicted s -process elemental contribution is correct, we have then obtained the total solar system abundances for those elements by summing N_s and $N_r(\text{predicted})$. Those values, along with $\log \varepsilon_{total}$, are also listed in Table 5.

While it is clear that we have made several simplifying assumptions in making these new predictions, several points are worth noting. In the case of Gd we find that the stellar data suggests a higher recommended value for the r -process contribution and total Solar System value. Interestingly, this total predicted value for Gd, $\log \varepsilon_{total} = 1.11$, is identical to our new measured photospheric abundance for this element. For Sm our predicted value, $\log \varepsilon_{total} = 1.00$, is also identical to the measured solar photospheric value (LDSC06) and for Ho our prediction, 0.53, is consistent with recent measured photospheric values $\log \varepsilon_{total} = 0.51 \pm 0.1$ (Lawler et al. 2004) and $\log \varepsilon_{total} = 0.53 \pm \approx 0.1$ (Bord & Cowley 2002). In the case of Nd, we find very little difference between the older predicted values and the new one based upon the stellar data. Our predicted solar abundance, $\log \varepsilon_{total} = 1.46$, is in very good agreement with both the meteoritic and photospheric values, including the recent photospheric measurement of $\log \varepsilon_{total} = 1.45 \pm 0.01$ by Den Hartog et al. (2003) and the recommendation of Lodders (2003) of 1.46 based upon the meteoritic measurements. Our analyses may suggest, at least for the cases of Gd, Sm and Ho, that the (slightly) higher photospheric determinations (including recent ones found by our group) might be the recommended solar values, or at least be more appropriate for stellar abundance studies, than the meteoritic ones.

We caution in this numerical analysis, however, that there are some inconsistencies in the data sources regarding the s -process contributions, which in turn effects the r -process residual abundances. Many of the s -process determinations, for instance, were obtained using older cross section measurements (Käppeler et al. 1989) and older Solar System abundance determinations (Anders & Grevesse 1984). The specific s -process (and r -process) contributions

are based upon individual isotopic neutron capture cross sections, and assume a specific s -process model - we have chosen to employ the “standard model”. Elemental abundance values are the then sum of the isotopic values. Since there are some uncertainties in the cross sections and in the assumed model predictions, these elemental sums sometime can have slight deviations from the predicted total solar values. In addition since that time, some of the cross sections (and hence s -process contributions) have been updated, as has the total Solar System abundance predictions (Lodders 2003). Thus, our precise (total) r -process abundance numerical values predicted for the Solar System have to be viewed with some caution, or at least with some error bars. Nevertheless, we think the general procedure is sound - that the halo stars abundances can be used to predict (or at least constrain) the Solar System r -process values - and the general trends suggest a revision may be needed in those current values. Clearly, a new systematic analysis of the s -process contributions (based upon new nuclear cross section experiments) needs to be performed on the latest solar system abundance determinations (Lodders 2003).

Many of other possible sources of systematic error were discussed in earlier sections. Most of these effects will shift the absolute r -process scale without changing the internal r -process pattern. The similarity of RE excitation and ionization potentials tends to “cancel out” effects from choosing a slightly different photospheric model or slightly different model parameters. The use of many metal lines in each abundance determination suppresses errors from blending and continuum placement during analysis of stellar data. The overall “scale” uncertainties on the laboratory transition probability data from the LIF radiative lifetime measurements are quite small as described in §2 and illustrated in LDSC06 with a more extensive comparison of independent sets of LIF measurements on Sm II. If the difficult radiometric calibrations of the FTS data needed for branching fraction measurements were seriously in error, then we would expect to see a wavelength dependence in the elemental abundances. Figure 4 is a crucial test for this systematic problem. Incomplete knowledge of RE energy levels and level assignments was a significant concern during our work on Sm II, but it was not a problem in the present work on Gd II. This is one systematic which could change the internal r -process pattern. If there were significant residuals, or long wavelength transitions to unobserved lower levels in Sm II, then the $\log(gf)$ values used in the Sm II abundance determinations would need to be decreased and the Sm abundances would increase. The net result would move the Sm abundances further above the solid line of Figure 5, which is not the direction needed to support the conventional r -process abundance pattern determined by subtracting calculated s -process abundances from the solar (photospheric) or solar system (meteoric) abundance pattern.

5.2 Isotopic Considerations for Gd II

Gadolinium has seven abundant naturally occurring isotopes: ^{152}Gd (0.2% of the solar-system elemental abundance), ^{154}Gd (2.2%), ^{155}Gd (14.8%), ^{156}Gd (20.5%), ^{157}Gd (15.6%), ^{158}Gd (24.8%), and ^{160}Gd (21.9%). We have listed

the values from both the standard and stellar models (Arlandini et al. 1999) in Table 6. The abundances for the s - and r -process contributions are based upon the $\text{Si} = 10^6$ scale (see Cowan et al. 2006). We have also listed the percentage contribution by individual isotope to the total elemental s - and r -process abundances (i.e., the vertical columns add up to 100% in those particular columns). It is clear from the table that both the standard and stellar models give very similar isotopic abundance predictions for each of the s - and r -process mixtures for Gd.

The widths of line profiles in our high resolution FTS data vary, and in a few cases the profiles have partially resolved structure. Although it is not possible today, it may at some point in the future be possible to observe the isotopic mixture of Gd in a metal-poor halo star, similarly to what Lambert & Allende Prieto (2002) have done for the element Ba in the halo star HD 140283. They determined that the fractional abundance of the odd isotopes of Ba

$$f_{\text{odd}} = [\text{N}(^{135}\text{Ba}) + \text{N}(^{137}\text{Ba})]/\text{N}(\text{Ba})$$

in this star was consistent with the solar system r -process isotopic ratio. Gd is an even- Z nucleus (like Ba and Sm) and has seven stable (s - and r -process admixed) isotopes. Thus, (similarly to Ba and Sm) we can define for Gd

$$f_{\text{odd}} = [\text{N}(^{155}\text{Gd}) + \text{N}(^{157}\text{Gd})]/\text{N}(\text{Gd}).$$

For the pure r -process components of solar system isotopic abundances, we find that $f_{\text{odd}}^r = 0.33$ employing values from either the standard model (Cowan et al. 2006) or the stellar model (Arlandini et al. 1999) that are listed in Table 6. Interestingly, this result for Gd is almost identical to the value (0.36) found for Sm (LDSC06). (Note that this result and the values listed in Table 6, come from the original prediction for the total r -process contribution to Gd, N_r , and not on the new suggested value discussed above.)

For comparison, the Gd solar s -process values are $f_{\text{odd}}^s = 0.16$ and $f_{\text{odd}}^s = 0.17$ for the standard and stellar models, respectively.

There have been very few stellar isotopic abundance observations. These include only the one measurement of Ba in HD 140283 by Lambert and Allende-Prieto and several Eu isotopic observations (Snedden et al. 2002, Aoki et al. 2003). An observation of the isotopic mixture for Gd in any halo star, would give important information about early Galactic nucleosynthesis. For example, such an observation of Gd (82% r -process), perhaps in conjunction with another element such as Sm (67% r -process in solar system material) in the same star, would provide a direct measure of the r -process contribution to the elemental Gd (and perhaps Sm) production in nucleosynthetic (e.g., supernovae) sites that were operating in the early Galaxy. Further, it would confirm that not only the elemental, but the isotopic abundances of these elements are consistent with the Solar System r -process distribution. Such observations would also be a measure of the “robustness” of the r -process (operating in approximately the same manner over many Gyr between the formation of the Galaxy and the Solar System) and a confirmation that the Solar System abundances are in many ways cosmic.

6. SUMMARY AND CONCLUSIONS

New LIF radiative lifetime measurements for 63 levels of Gd II and FTS branching fraction/atomic transition probability measurements for 611 transitions of Gd II were completed and reported herein. These laboratory measurements were applied to re-determine the Solar photospheric abundance of Gd, and to extend our effort to more sharply define a pure r -process abundance pattern using the metal-poor Galactic halo stars CS 22892-052, BD+17°3248, and HD 115444. A sharply defined r -process abundance pattern will provide a strong constraint for advanced models of this process.

We have employed the increasingly accurate stellar abundance determinations, resulting in large part from the more precise laboratory atomic data, to predict directly the Solar System r -process elemental abundances for Gd, Sm, Ho and Nd. Our analysis of the stellar data suggests slightly higher recommended values for the r -process contribution and total Solar System values. These values are consistent with recent photospheric determinations (including those from our group), for the elements Gd, Sm and Ho. This may suggest that these slightly higher photospheric values might be the recommended solar values, or at least be more appropriate for stellar abundance studies. Similarly to the case of Sm, we have analyzed the isotopic mixture of Gd providing some odd-isotope, and r -process ratio, predictions that could be utilized in future Gd isotopic studies. The combination of improved laboratory data, better observational data, and advanced models will unambiguously identify the site(s) of the r -process, and fully elucidate the role of the r -process in the chemical evolution of the Galaxy and the Universe.

ACKNOWLEDGMENTS

This work is supported by the National Science Foundation under grants AST-0506324 (JEL and EADH), AST0307495 (CS), and AST-0307279 (JJC). J. E. Lawler is a guest observer at the National Solar Observatory and he is indebted to Mike Dulick and Detrick Branstron for help with the 1 m Fourier transform spectrometer. We thank K. Lodders for helpful comments about the Solar System abundances.

REFERENCES

- Adams, D. L., & Whaling, W. 1981, *J. Opt. Soc. Am.*, 71, 1036
Aoki, W., Ryan, S. G., Iwamoto, N., Beers, T. C., Norris, J. E., Ando, H., Kajino, T., Mathews, G. J., & Fujimoto, M. Y. 2003, *ApJ*, 592, L67
Arlandini, C., Käppeler, F., Wisshak, K., Gallino, R., Lugaro, M., Busso, M., & Straniero, O. 1999, *ApJ*, 525, 886
Asplund, M., Grevesse, N., & Sauval, A. J. 2005, *ASP Conf. Ser.* 336: *Cosmic Abundances as Records of Stellar Evolution and Nucleosynthesis*, 336, 25
Bergström, H., Biémont, E., Lundberg, H., Persson, A. 1988, *A&A*, 192, 335.

- Biémont, E., Baudoux, M., Kurucz, R. L., Ansbacher, W., & Pinnington, E. H. 1991, *A&A*, 249, 539
- Biémont, E. & Quinet P. 2003, *Physica Scripta*, T105, 38
- Blaise, J., van Kleef, Th. A. M., Wyart, J. F. 1971, *J. de Phys.*, 32, 617
- Bord, D. J. & Cowley, C. R. 2002, *Sol. Phys.*, 211, 3
- Brault, J. W. 1976, *J. Opt. Soc. Am.*, 66, 1081
- Busso, M., Gallino, R., & Wasserburg, G. J. 1999, *ARA&A*, 37, 239
- Cayrel, R., et al., 2004, *A&A*, 416, 1117
- Corliss, C. H., & Bozman, W. R. 1962, *Experimental Transition Probabilities for Spectral Lines of Seventy Elements*, U. S. Natl. Bur. Standards Monograph 53, (Washington: U. S. Government Printing Office)
- Cowan, J. J., Burris, D. L., Sneden, C., McWilliam, A., & Preston, G. W. 1995, *ApJ*, 439, L51
- Cowan, J. J., Sneden, C., Burles, S., Ivans, I. I., Beers, T. C., Truran, J. W., Lawler, J. E., Primas, F., Fuller, G. M., Pfeiffer, B., & Kratz, K.-L. 2002, *ApJ*, 572, 861
- Cowan, J. J., & Thielemann, F.-K. 2004, *Phys. Today*, 57, 47
- Cowan, J. J., Lawler, J. E., Sneden, C., Den Hartog, E. A., & Collier, J. 2006, To appear in *Proc. 2006 NASA LAW ed. V. Kwong*
- Cowan, J. J., & Sneden, C. 2006, *Nature*, 440, 1151
- Cowan, R. D. 1981, *The Theory of Atomic Structure and Spectra* (Berkeley, Univ. of California Press) p 601
- Cowley, C. R. & Corliss, C. H. 1983, *MNRAS* 203, 651
- Danzmann, K., & Kock, M. 1982, *J. Opt. Soc. Am.*, 72, 1556
- Delbouille, L, Roland, G., & Neven, L. 1973, *Photometric Atlas of the Solar Spectrum from λ 3000 to λ 10000*, (Liège, Inst. D'Ap., Univ. de Liège)
- Den Hartog, E. A., Lawler, J. E., Sneden, C., & Cowan, J. J. 2003, *ApJS*, 148, 543
- Den Hartog, E. A., Wickliffe, M. E., & Lawler, J. E. 2002, *ApJS*, 141, 255
- Den Hartog, E. A., Wiese, L. M. & Lawler, J. E. 1999, *J. Opt. Soc. Am. B*, 16, 2278
- Edlén, B. 1953, *J. Opt. Soc. Am.*, 43, 339
- Gorshkov, V. N., & Komarovskii, V. A. 1986, *Sov. Astron.* 30, 333 [orig. 1986, *Astron. Zh.*, 63, 563],
- Gorshkov, V. N., Komarovskii, V. A., Osherovich, A. L., & Penkin, N. P. 1983, *Opt. Spectrosc. (USSR)*, 54, 122 [orig. 1983, *Opt. Spektrosk.* 54, 210]
- Gratton, R. G., & Sneden, C. 1994, *A&Ap*, 287, 927
- Grevesse, N., & Sauval, A. J. 1998, *Space Sci. Rev.*, 85, 161
- Grevesse, N., & Sauval, A. J. 1999, *A&A*, 347, 348
- Grevesse, N., & Sauval, A. J. 2002, *Adv. Space. Res.*, 30, 3
- Grigoriev, I. S., & Melikhov, E. Z. 1997, *Handbook of Physical Quantities*, (Boca Raton, CRC Press) p. 516
- Guo, B., Ansbacher, W., Pinnington, E. H., Ji, Q., & Berends, R. W. 1992, *Phys. Rev. A*, 46, 641
- Hannaford, P., Lowe, R. M., Grevesse, N., Biémont, E., & Whaling, W. 1982, *ApJ*, 261, 736

- Hashiguchi, S., & Hasikuni, M. 1985, *J. Phys. Soc. Japan* 54, 1290
- Holweger, H., & Müller, E. A. 1974, *Sol. Phys.*, 39, 19
- Irwin, A. W. 1981, *ApJS*, 45, 621
- Käppeler, F., Beer, H., & Wisshak, K. 1989, *Rep. Prog. Phys.*, 52, 945
- Kono, A., & Hattori, S. 1984, *Phys. Rev. A*, 29, 2981
- Kurucz, R. L. 1998, in *Fundamental Stellar Properties: The Interaction between Observation and Theory*, IAU Symp. 189, ed T. R. Bedding, A. J. Booth and J. Davis (Dordrecht: Kluwer), p. 217
- Lambert, D.L., & Allende Prieto, C. 2002, *MNRAS*, 335, 325
- Lawler, J. E., Bonvallet, G., & Sneden, C. 2001a, *ApJ*, 556, 452
- Lawler, J. E., Wickliffe, M. E., Den Hartog, E. A., & Sneden, C. 2001b, *ApJ*, 563, 1075
- Lawler, J. E., Wickliffe, M. E., Cowley, C. R., & Sneden, C. 2001c, *ApJS*, 137, 341
- Lawler, J. E., Sneden, C., & Cowan, J. J. 2004, *ApJ*, 604, 850
- Lawler, J. E., Den Hartog, E. A., Sneden, C., & Cowan, J. J. 2006, *ApJS*, 162, 227
- Lodders, K. 2003, *ApJ*, 591, 1220
- Malcheva, G., Blagoev, K., Mayo, R., Ortiz, M., Xu, H. L., Svanberg, S., Quinet, P., & Biémont, E. 2006, *MNRAS*, 367, 754
- Martin, W.C., Zalubas, R., & Hagan, L. 1978, *Atomic Energy Levels The Rare Earth Elements*, NSRDSNBS 60 (Washington: U. S. G. P. O.) p. 174
- Martin, W. C., Sugar, J., & Musgrove, A. 2000, NIST Atomic Spectra Database, (http://physics.nist.gov/cgi-bin/AtData/main_asd)
- McWilliam, A., Preston, G. W., Sneden, C., & Searle, L. 1995, *AJ*, 109, 2757
- Meggers, W. F., Corliss, C. H., and Scribner, B. F. 1961, *Tables of Spectral Line Intensities*, U. S. Natl. Bur. Standards Monograph 32, (Washington: U.S. G.P.O.)
- Meggers, W. F., Corliss, C. H., and Scribner, B. F. 1975, *Tables of Spectral Line Intensities*, U. S. Natl. Bur. Standards Monograph 145, (Washington: U.S. G. P. O.)
- Moore, C. E., Minnaert, M. G. J., & Houtgast, J. 1966, *The Solar Spectrum 2934 Å to 8770 Å*, NBS Monograph 61 (Washington: U.S. G. P. O.)
- Obbarius H. U., & Kock, M. 1982, *J. Phys. B: At. Mol. Opt. Phys.*, 15, 527
- O'Brien, S., Dababneh, S., Heil, M., Käppeler, F., Plag, R., Reifarth, R., Gallino, R., & Pignatari, M. 2003, *Phys. Rev. C*, 68, 035801
- Palmeri, P., Quinet, P., Wyart, J.-F., & Biémont, E. 2000, *Physica Scripta*, 61, 323
- Ryan, S. G., Norris, J. E., and Beers, T. C. 1996, *ApJ*, 471, 254
- Simmerer, J., Sneden, C., Cowan, J. J., Collier, J., Woolf, V. M., & Lawler, J. E. 2004, *ApJ*, 617, 1091
- Sneden, C. 1973, *ApJ*, 184, 839
- Sneden, C., et al., 2003, *ApJ*, 591, 936

- Sneden, C., McWilliam, A., Preston, G. W., Cowan, J. J., Burris, D. L., & Armosky, B. J. 1996, *ApJ*, 467, 819
- Sneden, C., Cowan, J. J., Lawler, J. E., Burles, S., Beers, T. C., Fuller, G. M. 2002, *ApJ* 566, L25
- Sneden, C., & Cowan, J. J. 2003, *Science*, 299, 70
- Truran, J. W., Cowan, J. J., Pilachowski, C. A., & Sneden, C. 2002, *PASP*, 114, 1293
- Volz, U., & Schmoranzner, H. 1998, in *AIP Conf. Proc. 434, Atomic and Molecular Data and Their Applications*, ed. P. J. Mohr and W. L. Wiese (Woodbury, NY:AIP), p. 67
- Ward, L. 1985, *Mon. Not. R. Astr. Soc.* 213, 17
- Weiss, A. W. 1995, *Phys. Rev. A*, 51, 1067
- Westin, J., Sneden, C., Gustafsson, B., & Cowan, J.J. 2000, *ApJ*, 530, 783
- Whaling, W., Carle, M. T., & Pitt, M. L. 1993, *J. Quant. Spectrosc. Radiat. Transfer* 50, 7
- Wickliffe, M. E., Lawler, J. E., & Nave, G. 2000, *J. Quant. Spectrosc. Radiat. Transfer*, 66, 363
- Wisshak, K., Voss, F., Käppeler, F., Kazakov, L., & Reffo, G. 1998, *Phys. Rev. C*, 57, 391
- Xu, H., Jiang, Z., & Svanberg, S. 2003, *J. Phys. B*, 36, 411
- Yan, Z-C, Tambasco, M., & Drake, G. W. F. 1998, *Phys. Rev. A*, 57, 1652
- Zhang, Z. G., Persson, A., Li, Z. S., Svanberg, S., & Zhankui, J. 2001a, *Eur. Phys. J. D*, 13, 301

FIGURE CAPTIONS

Figure 1: Partial Grotrian diagram for singly ionized Gd.

Figure 2: Relative transition strength factors, $\text{STR} \equiv \log(\varepsilon gf) - \theta_\chi$, for lines of Sm II (LDSC06) and Gd II (this study). For display purposes the long-wavelength limit has been set to 8000 Å, which cuts out only some extremely weak lines of Gd II and Sm II that can be detected neither in the Sun nor nearly all other stars. The short-wavelength limit of 2900 Å covers all lines at that end of the spectrum in these two studies. Definitions of “detection limit” and “strong lines” of these species are given in the text.

Figure 3: Representative Gd II lines at 4037.32 and 4037.89 Å (top panels (a) and (d)), 3549.36 Å (middle panels (b) and (e)), and 3358.63 Å (bottom panels (c) and (f)) in spectra of the Sun (left-hand panels (a), (b), and (c)) and the r -process-rich metal-poor giant BD+17°3248 (right-hand panels (d), (e), and (f)). In each panel there are four synthetic spectra drawn with solid lines. The synthetic spectrum with the weakest (sometimes totally absent) Gd II line was computed assuming no Gd contribution to the total absorption. For the other three syntheses, the middle-strength one was computed with the best-fit abundance to the Gd feature given in Table 4 (except for the 4037 Å pair, where the best compromise abundance between the two lines was used). The stronger/weaker syntheses surrounding the best-fit one were done assuming Gd abundances that were a factor of two larger/smaller. The filled circles represent the observed spectra. In the solar case, for display purposes we chose to plot the Delbouille et al. (1973) data at intervals of 0.01 Å instead of the original 0.002 Å.

Figure 4: Line-by-line Gd abundances for the Sun (x symbols) and the r -process-rich metal-poor giant stars BD+17°3248 (open circles), CS 22892-052 (plus signs), and HD 115444 (diamonds), plotted as a function of wavelength. For display purposes the long-wavelength end of the plot has been truncated at 4700 Å. This cuts just one line from the plot, that at 5733 Å, which was detected only in the solar spectrum. For each star, a dotted line is drawn at the mean abundance. As indicated in the figure legend, the three numbers in parentheses beside each star name are the mean abundance, the sample standard deviation σ , and the number of lines used in the analysis.

Figure 5. Neutron-capture elemental abundance patterns in CS 22892-052, HD 115444, and BD+17°3248 compared with the (scaled) Solar System r -process abundances (solid line) and the total Solar System meteoritic abundances recommended by Lodders (2003; dashed line). This figure is an update of Figure 13 in LDSC06. The abundance distributions of all of the stars have been normalized to that of Eu. In the top panel, stellar abundances are those reported in the original papers on these stars. In the bottom panel the comparisons are repeated for these stars, but substituting in the abundances of Nd,

Ho, and Sm, and now Gd derived in papers of this series. Also shown are solar photospheric abundances, with values of La, Nd, Sm, Eu, Gd, Tb, and Ho taken from this series, otherwise from Lodders (2003).

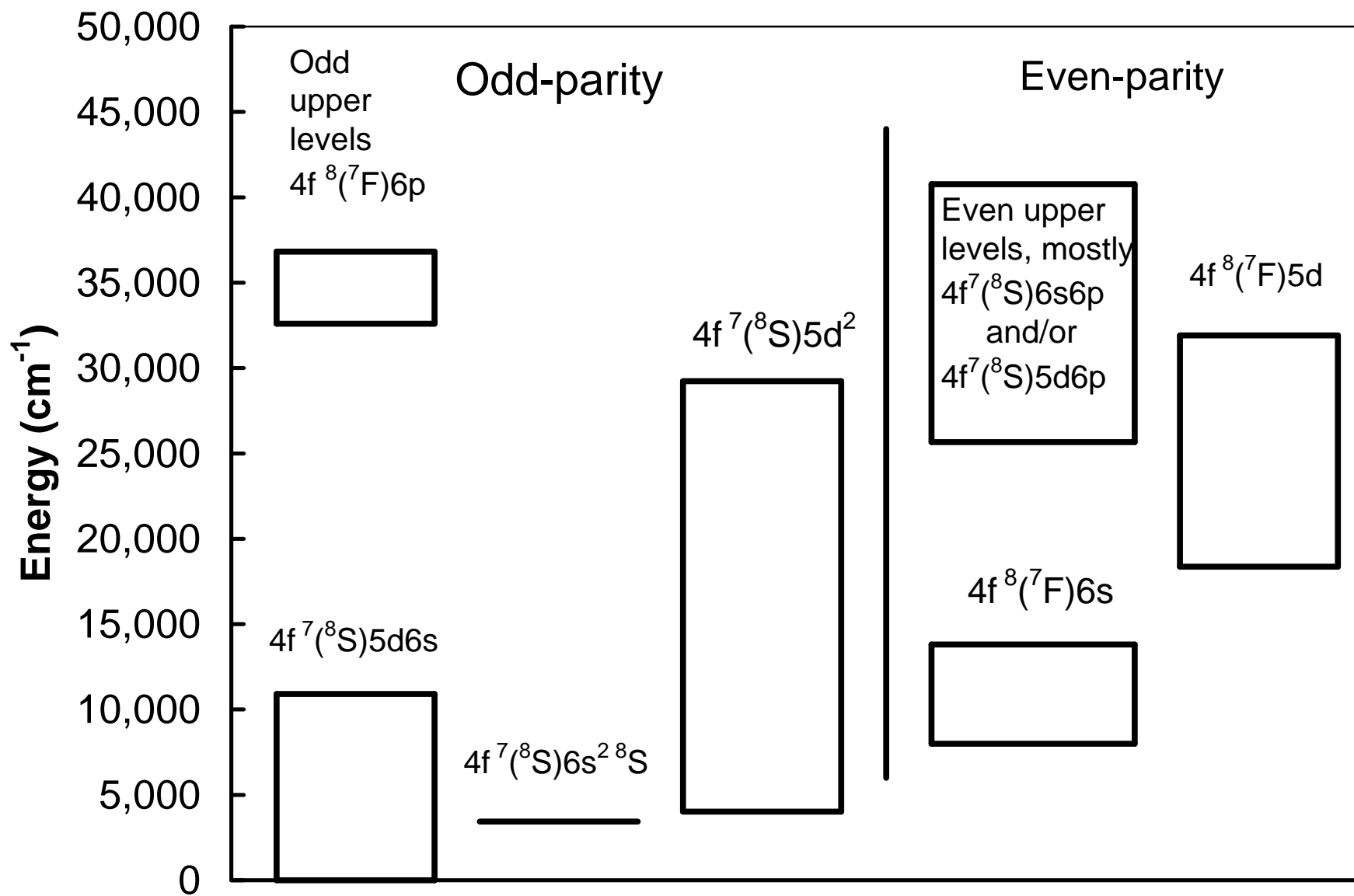


Table 1. Radiative lifetimes for Gd II levels from LIF measurements.

Level ^a (cm) ⁻¹	Parity ^b	Configuration ^a	Term ^a	J	Laser Wavelengths in Air (Å)	Lifetime (ns)		Ref for other lifetime
						This Expt ^c	Other	
25668.692	ev	4f ⁷ (⁸ S ^o)6s6p(³ P ^o)	¹⁰ P	3.5	3894.69, 3993.21	32.4		
25960.073	ev	4f ⁷ (⁸ S ^o)5d(⁹ D ^o)6p	¹⁰ F	1.5	3850.98, 4369.77	6.5	6.5±0.2	1
26211.912	ev	4f ⁷ (⁸ S ^o)5d(⁹ D ^o)6p	¹⁰ F	2.5	3813.98, 3852.46	6.4	6.4±0.3	1
26351.767	ev	4f ⁸ (⁵ D3)6s?	⁶ D?	4.5	3968.26, 4360.92	112		
26455.446	ev	4f ⁷ (⁸ S ^o)6s6p(³ P ^o)	¹⁰ P	4.5	3816.64, 4341.29	39.1		
26595.222	ev	4f ⁷ (⁸ S ^o)5d(⁹ D ^o)6p	¹⁰ F	3.5	3759.01, 4251.73	6.5	6.4±0.2	1
27162.224	ev	4f ⁷ (⁸ S ^o)5d(⁹ D ^o)6p	¹⁰ F	4.5	3768.40, 3844.58	6.3	6.1±0.3	1
27297.741	ev	4f ⁷ (⁸ S ^o)5d(⁹ D ^o)6p	¹⁰ D	2.5	3662.26, 4296.06	8.3		
27864.534	ev	4f ⁷ (⁸ S ^o)5d(⁹ D ^o)6p	¹⁰ F	5.5	4184.26, 4342.18	7.2		
27988.074	ev	4f ⁷ (⁸ S ^o)5d(⁹ D ^o)6p	¹⁰ D	3.5	3654.62, 4073.19	8.1		
28502.312	ev	4f ⁷ (⁸ S ^o)6s6p(³ P ^o)	¹⁰ P	5.5	3656.15, 4316.05	14.1	15.5±0.8	1
28629.017	ev	4f ⁸ (⁷ F)5d	⁸ P	2.5	4063.59, 4094.48	13.0		
29045.291	ev	4f ⁷ (⁸ S ^o)5d(⁹ D ^o)6p	¹⁰ D	4.5	3902.40, 4132.26	4.7	4.8±0.3	2
29197.887	ev	4f ⁷ (⁸ S ^o)5d(⁹ D ^o)6p		2.5	3454.91, 3971.75	11.0	12.3±0.6	1
29242.250	ev	4f ⁷ (⁸ S ^o)5d(⁹ D ^o)6p		3.5	3418.73, 4037.89	7.0	7.1±0.3	2
							6.3	3
29353.344	ev	4f ⁷ (⁸ S ^o)5d(⁹ D ^o)6p	¹⁰ F	6.5	3646.20, 4078.44	5.4	5.3±0.2	1
29877.937	ev	4f ⁷ (⁸ S ^o)5d(⁹ D ^o)6p	⁸ D	1.5	3345.99, 3730.85	4.7	4.7±0.3	2
29965.752	ev	4f ⁷ (⁸ S ^o)5d(⁹ D ^o)6p	⁸ D	2.5	3336.18, 3923.24	5.4	5.0±0.3	2
30008.894	ev	4f ⁷ (⁸ S ^o)5d(⁹ D ^o)6p	⁸ D	3.5	3331.39, 3839.64	4.9	5.0±0.3	2
							3.5	3
30027.378	ev	4f ⁷ (⁸ S ^o)5d(⁹ D ^o)6p	⁸ D	4.5	3358.62, 4049.42	4.5	4.5±0.2	1
30101.366	ev	4f ⁷ (⁸ S ^o)5d(⁹ D ^o)6p		5.5	4037.32, 4130.37	4.6	4.3±0.3	2
							4.3	3
30366.818	ev	4f ⁷ (⁸ S ^o)5d(⁹ D ^o)6p	¹⁰ D	5.5	3362.24, 3916.51	4.2	4.5±0.3	2
30849.648	ev	4f ⁷ (⁸ S ^o)6s6p(³ P ^o)	⁸ P	4.5	3268.33, 3645.62	14.7	14.6±0.5	2
30996.851	ev	4f ⁷ (⁸ S ^o)5d(⁹ D ^o)6p	¹⁰ D	6.5	3350.48, 4098.60	3.7	3.9±0.3	2
31145.651	ev	4f ⁷ (⁸ S ^o)5d(⁹ D ^o)6p	¹⁰ F	7.5	3422.46, 4073.75	4.6		
31908.123	ev	4f ⁷ (⁸ S ^o)6s6p(³ P ^o)	⁶ P	3.5	3133.09, 3512.22	12.8	11.9±0.5	2
32048.837	ev	4f ⁷ (⁸ S ^o)5d(⁹ D ^o)6p	⁸ F	1.5	3424.60, 3451.24	5.4		

Table 1—Continued

Level ^a (cm) ⁻¹	Parity ^b	Configuration ^a	Term ^a	J	Laser Wavelengths in Air (Å)	Lifetime (ns)		Ref for other lifetime
						This Expt ^c	Other	
32150.143	ev	4f ⁷ (⁸ S ^o)5d(⁹ D ^o)6p	⁸ F	2.5	3439.21, 3482.61	5.2	5.1±0.3	2
32260.120	ev	4f ⁷ (⁸ S ^o)5d(⁹ D ^o)6p		2.5	3399.99, 3467.27	5.2	5.5±0.3	2
32262.787	ev	4f ⁷ (⁸ S ^o)5d(⁹ D ^o)6p	⁸ F	3.5	3425.93, 3468.99	5.2	5.4±0.3	2
32304.409	ev	4f ⁷ (⁸ S ^o)5d(⁹ D ^o)6p		4.5	3119.94, 3156.54	4.8	4.8±0.3	2
32490.510	ev	4f ⁷ (⁸ S ^o)5d(⁹ D ^o)6p		3.5	3439.79, 3505.51	5.1	4.8±0.3	2
32595.348	od	4f ⁸ (⁷ F ₆)6p _{1/2}	(6,1/2) ^o	5.5	4063.38, 4253.60	9.0		
32677.540	od	4f ⁸ (⁷ F ₆)6p _{1/2}	(6,1/2) ^o	6.5	4049.85, 4238.78	7.8		
32684.712	ev	4f ⁷ (⁸ S ^o)5d(⁹ D ^o)6p	⁸ F	4.5	3416.95, 3481.80	5.4		
32946.196	ev	4f ⁷ (⁸ S ^o)5d(⁹ D ^o)6p	⁸ F	5.5	3450.38, 3557.06	5.0	4.7±0.3	2
33211.481	ev	4f ⁷ (⁸ S ^o)5d(⁹ D ^o)6p	¹⁰ P	3.5	3010.13, 3034.05	2.50	2.1±0.2	2
33557.951	ev	4f ⁷ (⁸ S ^o)5d(⁹ D ^o)6p	⁸ F	6.5	3161.38, 3481.28	5.0	4.7±0.3	2
33596.027	ev	4f ⁷ (⁸ S ^o)5d(⁹ D ^o)6p	¹⁰ P	4.5	2999.05, 3082.00	2.30	2.5±0.2	2
34108.475	od	4f ⁸ (⁷ F ₅)6p _{1/2}	(5,1/2) ^o	4.5	3996.31, 4137.10	10.0		
34178.776	ev	4f ⁷ (⁸ S ^o)5d(⁹ D ^o)6p	¹⁰ P	5.5	3027.60, 3100.50	2.20	2.5±0.2	2
34608.122	od	4f ⁸ (⁷ F ₅)6p _{1/2}	(5,1/2) ^o	5.5	4053.29, 4111.43	9.0		
34900.473	od	4f ⁸ (⁷ F ₄)6p _{1/2}	(4,1/2) ^o	3.5	4062.59, 4243.84	9.7		
35111.830	od	4f ⁸ (⁷ F ₆)6p _{3/2}	(6,3/2) ^o	6.5	3686.33, 3842.21	10.7		
35272.546	od	4f ⁸ (⁷ F ₆)6p _{3/2}	(6,3/2) ^o	7.5	3664.61	6.7		
35362.630	od			6.5	3652.55, 3805.52	15.5		
35605.266	od	4f ⁸ (⁷ F ₆)6p _{3/2}	(6,3/2) ^o	5.5	3620.45, 3770.70, 3895.79	8.0		
35822.697	od			4.5	3740.02, 3863.05	17.9		
36461.156	ev	4f ⁷ (⁸ S ^o)5d(⁷ D ^o)6p	⁸ D	5.5	3077.07, 3791.17	5.1		
36647.241	ev	4f ⁷ (⁸ S ^o)5d(⁷ D ^o)6p	⁸ D	4.5	3143.14, 3558.18	4.1		
36723.695	od	4f ⁸ (⁷ F ₅)6p _{3/2}	(5,3/2) ^o	5.5	3733.08, 3782.34	7.0		
36778.403	od			4.5	3610.92	15.4		
36821.816	od	4f ⁸ (⁷ F ₅)6p _{3/2}	(5,3/2) ^o	6.5	3605.26, 3719.45	7.2		
36845.366	ev	4f ⁷ (⁸ S ^o)5d(⁷ D ^o)6p	⁸ D	2.5	3608.76, 3649.44	4.1		
38010.603	od			5.5	3330.34	13.7		
38029.848	ev	4f ⁷ (⁸ S ^o)5d(⁷ D ^o)6p		4.5	3617.17	7.9		
38553.210	ev	4f ⁷ (⁸ S ^o)5d(⁷ D ^o)6p	⁶ F	5.5	3332.13	4.8		

Table 1—Continued

Level ^a (cm) ⁻¹	Parity ^b	Configuration ^a	Term ^a	J	Laser Wavelengths in Air (Å)	Lifetime (ns)		Ref for other lifetime
						This Expt ^c	Other	
38628.604	ev			2.5	2794.66, 2841.34	5.4		
39024.491	ev	4f ⁷ (⁸ S ^o)5d(⁷ D ^o)6p	⁸ P	2.5	2781.40, 2809.72	2.45	2.34±0.2	1
39170.192	ev	4f ⁷ (⁸ S ^o)5d(⁷ D ^o)6p	⁸ P	3.5	2770.17, 2840.23	2.55	2.34±0.2	1
39250.737	ev	4f ⁷ (⁸ S ^o)5d(⁷ D ^o)6p	⁶ F	4.5	2791.97, 2833.75	3.2		
39537.159	ev	4f ⁷ (⁸ S ^o)5d(⁷ D ^o)6p	⁸ P	4.5	2769.81, 2881.33	3.2	3.12±0.2	1
40773.207	ev	4f ⁷ (⁸ S ^o)5d(⁷ D ^o)6p	⁸ F	6.5	3102.55	4.3		

^aEnergy levels, configurations, and terms are from Martin et al. (1978).

^bThe even-parity (ev) and odd-parity (od) notation introduced here is used in Table 3, our main table of transition probabilities.

^cThe uncertainty of our measurements is the larger of ±5% or ±0.2 ns.

References for other LIF lifetime measurements: (1) Xu, H., Jiang, Z., & Svanberg, S. 2003, J. Phys. B, 36, 411; (2) Zhang, Z. G., Persson, A., Li, Z. S., Svanberg, S., & Zhankui, J. 2001, Eur. Phys. J. D, 13, 301; (3) Bergström, H., Biémont, E., Lundberg, H., Persson, A. 1988, A&A, 192, 335.

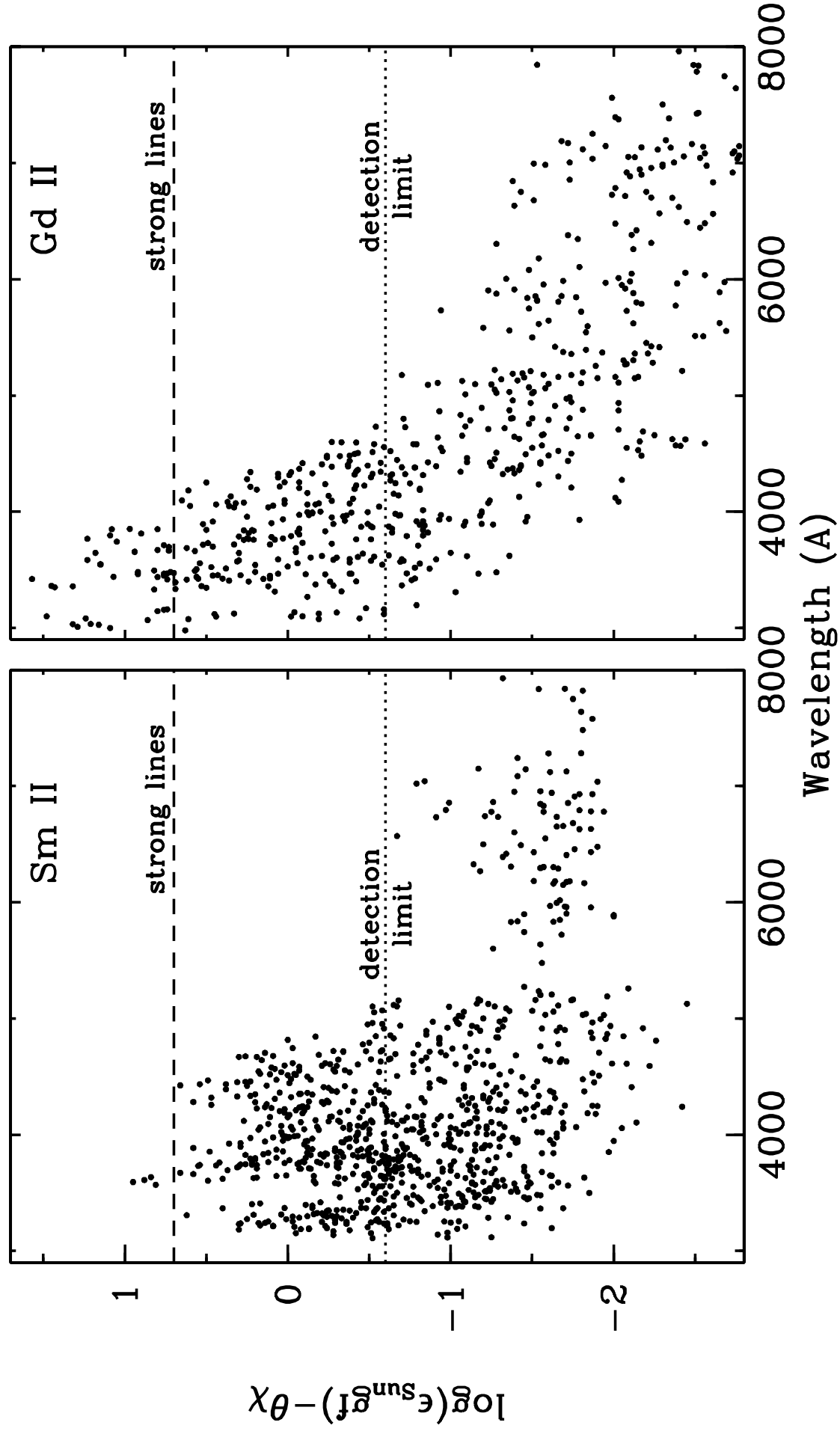


Table 2. Fourier transform spectra of Gd lamps used in this study. All were recorded using the 1 m FTS on the McMath telescope at the National Solar Observatory, Kitt Peak, AZ.

Index	Date	Serial No.	Lamp Type ¹	Buffer Gas	Lamp Current (mA)	Wavenumber Range (cm ⁻¹)	Limit of Resolution (cm ⁻¹)	Coadds	Beam Splitter	Filter	Detector ²	Calibration ³
1	2002 Feb. 27	18	Commercial HCD	Ar	26	7929 – 34998	0.050	50	UV		S. B. Si Diode	Ar I & II WQH Lamp
2	2000 Feb. 28	23	Commercial HCD	Ar	23	7929 – 34998	0.053	16	UV		S. B. Si Diode	Ar I & II
3	2000 Feb. 27	18	Commercial HCD	Ar	30	7929 – 34998	0.053	41	UV		S. B. Si Diode	Ar I & II
4	2001 Feb. 27	19	Commercial HCD	Ar	15	7929 – 34998	0.053	9	UV		S. B. Si Diode	Ar I & II
5	2002 Feb. 27	20	Commercial HCD	Ar	12.5	7929 – 34998	0.053	9	UV		S. B. Si Diode	Ar I & II
6	1991 Oct. 10	13	Custom HCD	Ar	295	15154 - 36081	0.044	4	UV	CuSO ₄	S. B. Si Diode	Ar I & II W Strip Lamp
7	1991 Oct. 10	14	Custom HCD	Ar	290	15154 - 36081	0.044	4	UV	CuSO ₄	S. B. Si Diode	Ar I & II W Strip Lamp
8	1991 Oct. 9	11	Custom HCD	Ar	300	7810 – 25033	0.031	4	UV	GG 495	S. B. Si Diode	W Strip Lamp
9	1991 Oct. 9	12	Custom HCD	Ar	300	7810 – 25033	0.031	4	UV	GG 495	S. B. Si Diode	W Strip Lamp
10	1991 Dec. 12	7	Custom HCD	Ar	300	1661 – 11312	0.015	8	CaF ₂	GaAs	InSb	Ar I & II W Strip Lamp
11	1991 Dec. 12	8	Custom HCD	Ne	300	1661 – 11312	0.015	8	CaF ₂	GaAs	InSb	W Strip Lamp
12	2001 Jan. 25	13	Commercial HCD	Ne	25	7929 - 34998	0.050	10	UV		S. B. Si Diode	
13	2001 Jan. 26	15	Commercial HCD	Ne	20	7929 – 34998	0.050	10	UV		S. B. Si Diode	
14	1985 Feb. 6	10	EDL	Ar		7456 – 28808	0.035	2	UV	GG 375	S. B. Si Diode	W Strip Lamp
15	1985 Feb. 6	67	EDL	Ar		7456 – 28808	0.035	8	UV	GG 375	S. B. Si Diode	W Strip Lamp
16	1985 Feb. 6	89	EDL	Ar		3285 – 15050	0.018	8	UV	RG 715	InSb	W Strip Lamp

¹Lamp types include commercially available small sealed Hollow Cathode Discharge (HCD) lamps typically used in atomic absorption spectrophotometers, a custom water-cooled HCD lamp, and an Electrodeless Discharge Lamp (EDL).

²Detectors types include the Super Blue (S. B.) Si photodiode.

³Relative radiometric calibrations were based on selected sets of Ar I and Ar II lines, on a Tungsten-Quartz-Halogen (WQH) lamp calibrated as a secondary irradiance standard, and on a Tungsten (W) Strip Lamp calibrated as a secondary radiance standard.

Sun

BD+17°3248

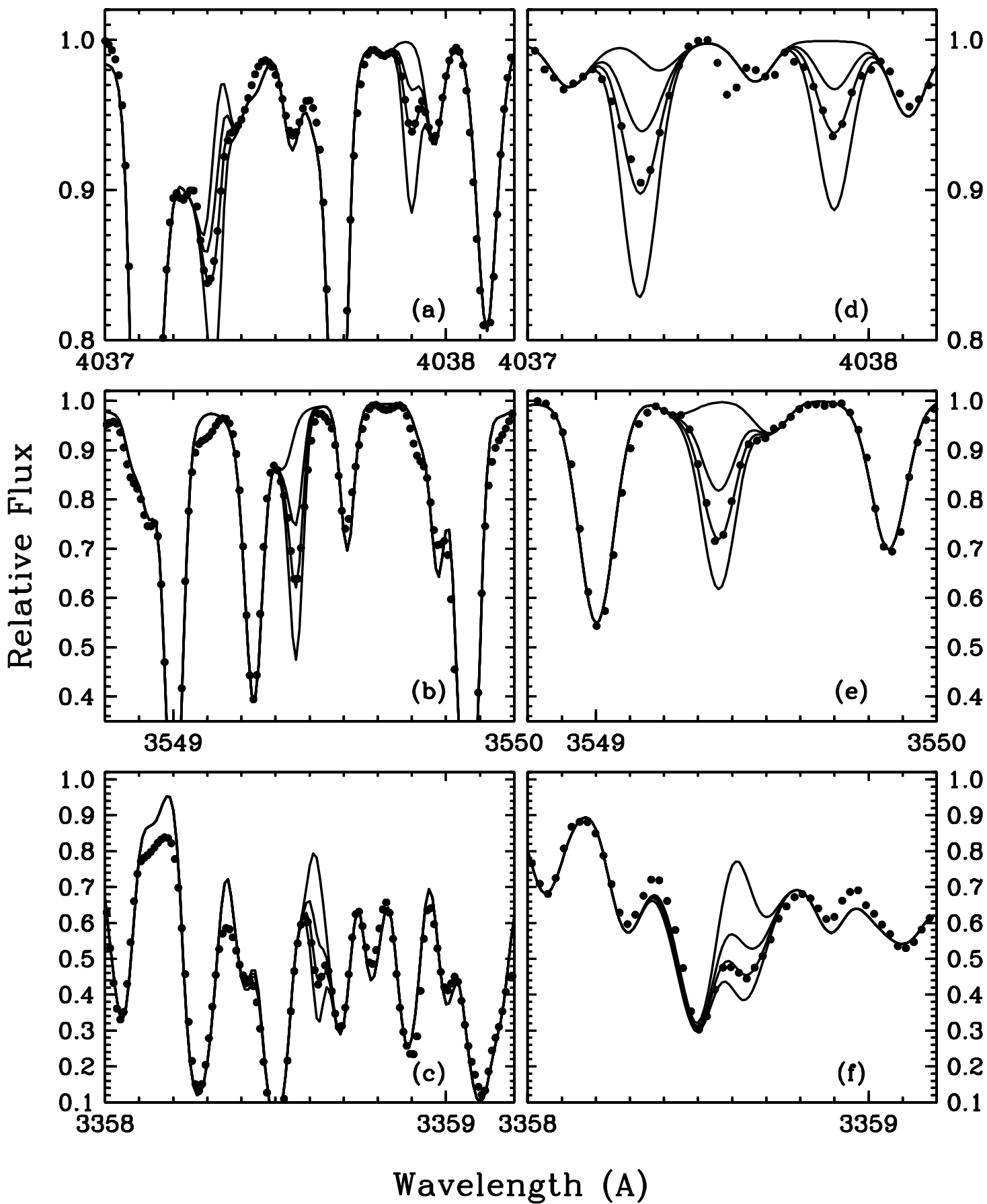


Table 3. Atomic transition probabilities for Gd II organized by increasing wavelength in air, λ_{air} .

λ_{air} (Å)	E_{upper} (cm^{-1})	Parity	J_{upp}	E_{lower} (cm^{-1})	Parity	J_{low}	A-value (10^6 s^{-1})	$\text{Log}(gf)$
2980.156	34178.776	ev	5.5	633.273	od	4.5	26 ± 3	-0.39
2999.049	33596.027	ev	4.5	261.841	od	3.5	77 ± 9	0.02
3010.130	33211.481	ev	3.5	0.000	od	2.5	141 ± 12	0.19
3027.601	34178.776	ev	5.5	1158.943	od	5.5	96 ± 10	0.20
3032.844	33596.027	ev	4.5	633.273	od	4.5	144 ± 13	0.30
3034.051	33211.481	ev	3.5	261.841	od	3.5	124 ± 10	0.14
3068.645	33211.481	ev	3.5	633.273	od	4.5	62 ± 5	-0.16
3076.928	32490.510	ev	3.5	0.000	od	2.5	28.6 ± 2.6	-0.49
3077.072	36461.156	ev	5.5	3972.167	od	4.5	9.4 ± 1.7	-0.80
3081.996	33596.027	ev	4.5	1158.943	od	5.5	135 ± 12	0.28
3083.347	32684.712	ev	4.5	261.841	od	3.5	2.2 ± 0.4	-1.51
3098.647	32262.787	ev	3.5	0.000	od	2.5	18.8 ± 1.6	-0.66
3098.903	32260.120	ev	2.5	0.000	od	2.5	8.8 ± 0.9	-1.12
3100.504	34178.776	ev	5.5	1935.310	od	6.5	241 ± 22	0.62
3101.927	32490.510	ev	3.5	261.841	od	3.5	6.0 ± 0.7	-1.16
3119.080	32684.712	ev	4.5	633.273	od	4.5	1.70 ± 0.30	-1.61
3119.944	32304.409	ev	4.5	261.841	od	3.5	16.5 ± 1.1	-0.62
3124.002	32262.787	ev	3.5	261.841	od	3.5	15.4 ± 1.0	-0.74
3124.262	32260.120	ev	2.5	261.841	od	3.5	6.3 ± 0.7	-1.26
3133.090	31908.123	ev	3.5	0.000	od	2.5	3.39 ± 0.29	-1.40
3135.038	32150.143	ev	2.5	261.841	od	3.5	8.8 ± 1.0	-1.11
3145.004	32946.196	ev	5.5	1158.943	od	5.5	39 ± 3	-0.16
3156.535	32304.409	ev	4.5	633.273	od	4.5	36.7 ± 3.0	-0.26
3160.689	32262.787	ev	3.5	633.273	od	4.5	2.1 ± 0.3	-1.61
3161.376	33557.951	ev	6.5	1935.310	od	6.5	36.2 ± 2.2	-0.12
3171.091	32684.712	ev	4.5	1158.943	od	5.5	2.4 ± 0.3	-1.44
3196.533	31908.123	ev	3.5	633.273	od	4.5	1.27 ± 0.17	-1.81
3268.334	30849.648	ev	4.5	261.841	od	3.5	4.0 ± 0.4	-1.19
3308.511	30849.648	ev	4.5	633.273	od	4.5	0.54 ± 0.11	-2.05
3313.734	33596.027	ev	4.5	3427.274	od	3.5	15 ± 3	-0.60
3315.598	33596.027	ev	4.5	3444.235	od	3.5	6.1 ± 1.2	-1.00

Table 3—Continued

λ_{air} (Å)	E_{upper} (cm^{-1})	Parity	J_{upp}	E_{lower} (cm^{-1})	Parity	J_{low}	A-value (10^6 s^{-1})	$\text{Log}(gf)$
3331.387	30008.894	ev	3.5	0.000	od	2.5	39.6 ± 2.8	-0.28
3336.184	29965.752	ev	2.5	0.000	od	2.5	38.9 ± 2.6	-0.41
3345.989	29877.937	ev	1.5	0.000	od	2.5	37 ± 3	-0.60
3350.478	30996.851	ev	6.5	1158.943	od	5.5	124 ± 7	0.47
3358.432	33211.481	ev	3.5	3444.235	od	3.5	20.8 ± 2.7	-0.55
3358.625	30027.378	ev	4.5	261.841	od	3.5	105 ± 5	0.25
3360.712	30008.894	ev	3.5	261.841	od	3.5	21.0 ± 1.7	-0.54
3362.239	30366.818	ev	5.5	633.273	od	4.5	133 ± 7	0.43
3365.593	29965.752	ev	2.5	261.841	od	3.5	4.3 ± 0.5	-1.35
3367.090	30849.648	ev	4.5	1158.943	od	5.5	1.29 ± 0.17	-1.66
3374.688	33596.027	ev	4.5	3972.167	od	4.5	9.8 ± 1.6	-0.78
3392.527	30101.366	ev	5.5	633.273	od	4.5	22.7 ± 1.5	-0.33
3399.402	32490.510	ev	3.5	3082.011	od	2.5	7.6 ± 0.8	-0.98
3399.987	32260.120	ev	2.5	2856.678	od	1.5	29.6 ± 2.0	-0.51
3401.067	30027.378	ev	4.5	633.273	od	4.5	2.1 ± 0.3	-1.44
3407.609	34178.776	ev	5.5	4841.106	od	5.5	34 ± 4	-0.14
3412.752	32150.143	ev	2.5	2856.678	od	1.5	3.0 ± 0.5	-1.51
3416.954	32684.712	ev	4.5	3427.274	od	3.5	49.4 ± 2.6	-0.06
3418.729	29242.250	ev	3.5	0.000	od	2.5	31.3 ± 1.7	-0.36
3422.464	31145.651	ev	7.5	1935.310	od	6.5	184 ± 9	0.71
3422.753	30366.818	ev	5.5	1158.943	od	5.5	7.3 ± 0.7	-0.81
3423.924	29197.887	ev	2.5	0.000	od	2.5	26.5 ± 1.4	-0.55
3424.595	32048.837	ev	1.5	2856.678	od	1.5	63 ± 3	-0.35
3425.931	32262.787	ev	3.5	3082.011	od	2.5	17.5 ± 1.1	-0.61
3426.244	32260.120	ev	2.5	3082.011	od	2.5	3.0 ± 0.5	-1.50
3439.208	32150.143	ev	2.5	3082.011	od	2.5	112 ± 6	0.08
3439.787	32490.510	ev	3.5	3427.274	od	3.5	54 ± 3	-0.12
3439.988	30996.851	ev	6.5	1935.310	od	6.5	65 ± 4	0.21
3449.618	29242.250	ev	3.5	261.841	od	3.5	7.7 ± 0.5	-0.96
3450.378	32946.196	ev	5.5	3972.167	od	4.5	66 ± 4	0.15
3451.236	32048.837	ev	1.5	3082.011	od	2.5	78 ± 4	-0.26

Table 3—Continued

λ_{air} (Å)	E_{upper} (cm^{-1})	Parity	J_{upp}	E_{lower} (cm^{-1})	Parity	J_{low}	A-value (10^6 s^{-1})	$\text{Log}(gf)$
3454.146	30101.366	ev	5.5	1158.943	od	5.5	9.9 ± 0.6	-0.67
3454.907	29197.887	ev	2.5	261.841	od	3.5	21.2 ± 1.1	-0.64
3461.956	32304.409	ev	4.5	3427.274	od	3.5	6.8 ± 0.5	-0.91
3462.999	30027.378	ev	4.5	1158.943	od	5.5	4.7 ± 0.5	-1.07
3463.990	32304.409	ev	4.5	3444.235	od	3.5	100 ± 5	0.25
3466.498	34178.776	ev	5.5	5339.477	od	5.5	6.9 ± 1.1	-0.83
3466.953	32262.787	ev	3.5	3427.274	od	3.5	16.5 ± 1.0	-0.62
3467.274	32260.120	ev	2.5	3427.274	od	3.5	112 ± 6	0.08
3467.670	36821.816	od	6.5	7992.268	ev	6.5	2.10 ± 0.30	-1.28
3468.084	31908.123	ev	3.5	3082.011	od	2.5	5.6 ± 0.3	-1.10
3468.994	32262.787	ev	3.5	3444.235	od	3.5	82 ± 4	0.07
3469.315	32260.120	ev	2.5	3444.235	od	3.5	3.7 ± 0.5	-1.40
3473.224	29045.291	ev	4.5	261.841	od	3.5	23.7 ± 1.4	-0.37
3479.513	36723.695	od	5.5	7992.268	ev	6.5	1.9 ± 0.4	-1.39
3481.280	33557.951	ev	6.5	4841.106	od	5.5	103 ± 5	0.42
3481.802	32684.712	ev	4.5	3972.167	od	4.5	72 ± 4	0.11
3482.607	32150.143	ev	2.5	3444.235	od	3.5	31.1 ± 1.7	-0.47
3491.960	28629.017	ev	2.5	0.000	od	2.5	26.9 ± 1.4	-0.53
3494.406	29242.250	ev	3.5	633.273	od	4.5	42.6 ± 2.2	-0.20
3505.512	32490.510	ev	3.5	3972.167	od	4.5	60 ± 3	-0.05
3510.127	31908.123	ev	3.5	3427.274	od	3.5	1.92 ± 0.22	-1.55
3512.219	31908.123	ev	3.5	3444.235	od	3.5	34.5 ± 1.8	-0.29
3518.631	29045.291	ev	4.5	633.273	od	4.5	0.85 ± 0.13	-1.80
3524.194	28629.017	ev	2.5	261.841	od	3.5	22.4 ± 1.2	-0.60
3528.539	32304.409	ev	4.5	3972.167	od	4.5	13.0 ± 0.8	-0.61
3542.765	33557.951	ev	6.5	5339.477	od	5.5	21.7 ± 1.4	-0.24
3544.978	32684.712	ev	4.5	4483.854	od	3.5	4.0 ± 0.4	-1.12
3545.790	29353.344	ev	6.5	1158.943	od	5.5	58 ± 3	0.19
3549.359	30101.366	ev	5.5	1935.310	od	6.5	85 ± 4	0.29
3554.795	32150.143	ev	2.5	4027.161	od	1.5	3.4 ± 0.4	-1.41
3557.058	32946.196	ev	5.5	4841.106	od	5.5	48.3 ± 2.9	0.04

Table 3—Continued

λ_{air} (Å)	E_{upper} (cm^{-1})	Parity	J_{upp}	E_{lower} (cm^{-1})	Parity	J_{low}	A-value (10^6 s^{-1})	$\text{Log}(gf)$
3558.476	32946.196	ev	5.5	4852.304	od	4.5	12.0 ± 0.7	-0.56
3564.041	32262.787	ev	3.5	4212.756	od	2.5	7.2 ± 0.5	-0.96
3569.561	32490.510	ev	3.5	4483.854	od	3.5	3.86 ± 0.30	-1.23
3571.931	27988.074	ev	3.5	0.000	od	2.5	10.5 ± 0.6	-0.79
3578.411	32150.143	ev	2.5	4212.756	od	2.5	4.5 ± 0.5	-1.29
3578.595	31908.123	ev	3.5	3972.167	od	4.5	5.0 ± 0.3	-1.12
3581.909	36461.156	ev	5.5	8551.049	od	5.5	78 ± 4	0.26
3584.961	29045.291	ev	4.5	1158.943	od	5.5	96 ± 5	0.27
3587.187	28502.312	ev	5.5	633.273	od	4.5	2.18 ± 0.14	-1.30
3590.464	32684.712	ev	4.5	4841.106	od	5.5	18.9 ± 1.2	-0.44
3591.435	32048.837	ev	1.5	4212.756	od	2.5	4.1 ± 0.4	-1.49
3591.909	32684.712	ev	4.5	4852.304	od	4.5	3.25 ± 0.30	-1.20
3593.439	32304.409	ev	4.5	4483.854	od	3.5	6.2 ± 0.4	-0.92
3605.262	36821.816	od	6.5	9092.491	ev	5.5	19.5 ± 1.3	-0.27
3605.664	27988.074	ev	3.5	261.841	od	3.5	4.0 ± 0.3	-1.21
3610.915	36778.403	od	4.5	9092.491	ev	5.5	20.5 ± 1.2	-0.40
3614.208	33557.951	ev	6.5	5897.264	od	6.5	4.5 ± 0.5	-0.90
3618.065	36723.695	od	5.5	9092.491	ev	5.5	3.7 ± 0.4	-1.07
3620.451	35605.266	od	5.5	7992.268	ev	6.5	20.4 ± 1.1	-0.32
3621.274	32946.196	ev	5.5	5339.477	od	5.5	0.67 ± 0.12	-1.80
3625.262	36461.156	ev	5.5	8884.809	od	4.5	10.1 ± 1.1	-0.62
3640.185	32304.409	ev	4.5	4841.106	od	5.5	5.5 ± 0.4	-0.96
3645.618	30849.648	ev	4.5	3427.274	od	3.5	21.1 ± 1.1	-0.38
3646.195	29353.344	ev	6.5	1935.310	od	6.5	75 ± 4	0.32
3647.875	30849.648	ev	4.5	3444.235	od	3.5	1.06 ± 0.11	-1.67
3652.546	35362.630	od	6.5	7992.268	ev	6.5	24.5 ± 1.3	-0.16
3654.624	27988.074	ev	3.5	633.273	od	4.5	52.4 ± 2.7	-0.08
3656.152	28502.312	ev	5.5	1158.943	od	5.5	39.7 ± 2.0	-0.02
3662.264	27297.741	ev	2.5	0.000	od	2.5	24.4 ± 1.3	-0.53
3664.608	35272.546	od	7.5	7992.268	ev	6.5	130 ± 7	0.62
3671.205	27864.534	ev	5.5	633.273	od	4.5	25.0 ± 1.4	-0.22

Table 3—Continued

λ_{air} (Å)	E_{upper} (cm^{-1})	Parity	J_{upp}	E_{lower} (cm^{-1})	Parity	J_{low}	A-value (10^6 s^{-1})	$\text{Log}(gf)$
3686.326	35111.830	od	6.5	7992.268	ev	6.5	24.1 ± 1.4	-0.16
3687.752	29965.752	ev	2.5	2856.678	od	1.5	60 ± 3	-0.13
3697.733	27297.741	ev	2.5	261.841	od	3.5	37.3 ± 1.9	-0.34
3699.737	29877.937	ev	1.5	2856.678	od	1.5	62 ± 3	-0.29
3709.135	33557.951	ev	6.5	6605.154	od	7.5	2.89 ± 0.21	-1.08
3712.704	30008.894	ev	3.5	3082.011	od	2.5	66 ± 3	0.04
3716.362	27162.224	ev	4.5	261.841	od	3.5	13.7 ± 0.8	-0.55
3719.452	36821.816	od	6.5	9943.779	ev	5.5	100 ± 5	0.46
3719.529	30849.648	ev	4.5	3972.167	od	4.5	15.4 ± 0.8	-0.50
3725.469	36778.403	od	4.5	9943.779	ev	5.5	34.5 ± 1.8	-0.14
3730.850	29877.937	ev	1.5	3082.011	od	2.5	70 ± 4	-0.23
3733.080	36723.695	od	5.5	9943.779	ev	5.5	44.1 ± 2.4	0.04
3743.470	27864.534	ev	5.5	1158.943	od	5.5	48.4 ± 2.5	0.09
3758.316	30027.378	ev	4.5	3427.274	od	3.5	18.5 ± 1.5	-0.41
3759.006	26595.222	ev	3.5	0.000	od	2.5	7.7 ± 0.4	-0.89
3760.714	30027.378	ev	4.5	3444.235	od	3.5	12.2 ± 0.9	-0.59
3762.999	28502.312	ev	5.5	1935.310	od	6.5	1.69 ± 0.10	-1.37
3763.331	30008.894	ev	3.5	3444.235	od	3.5	4.7 ± 0.6	-1.09
3767.043	29965.752	ev	2.5	3427.274	od	3.5	28.1 ± 1.5	-0.44
3768.396	27162.224	ev	4.5	633.273	od	4.5	76 ± 4	0.21
3769.452	29965.752	ev	2.5	3444.235	od	3.5	17.8 ± 1.1	-0.64
3770.695	35605.266	od	5.5	9092.491	ev	5.5	74 ± 4	0.28
3782.343	36723.695	od	5.5	10292.567	ev	4.5	74 ± 4	0.28
3787.571	30366.818	ev	5.5	3972.167	od	4.5	19.0 ± 1.4	-0.31
3791.171	36461.156	ev	5.5	10091.567	od	4.5	52.2 ± 2.9	0.13
3791.716	30849.648	ev	4.5	4483.854	od	3.5	2.49 ± 0.17	-1.27
3795.255	29197.887	ev	2.5	2856.678	od	1.5	2.02 ± 0.17	-1.58
3796.384	26595.222	ev	3.5	261.841	od	3.5	61 ± 3	0.02
3805.523	35362.630	od	6.5	9092.491	ev	5.5	30.1 ± 1.6	-0.04
3813.977	26211.912	ev	2.5	0.000	od	2.5	48.4 ± 2.5	-0.20
3816.643	26455.446	ev	4.5	261.841	od	3.5	6.8 ± 0.4	-0.83

Table 3—Continued

λ_{air} (Å)	E_{upper} (cm^{-1})	Parity	J_{upp}	E_{lower} (cm^{-1})	Parity	J_{low}	A-value (10^6 s^{-1})	$\text{Log}(gf)$
3821.511	29242.250	ev	3.5	3082.011	od	2.5	1.51 ± 0.10	-1.58
3822.167	30996.851	ev	6.5	4841.106	od	5.5	2.35 ± 0.27	-1.14
3826.050	30101.366	ev	5.5	3972.167	od	4.5	8.2 ± 0.6	-0.67
3831.810	26351.767	ev	4.5	261.841	od	3.5	2.29 ± 0.14	-1.30
3836.915	30027.378	ev	4.5	3972.167	od	4.5	17.8 ± 1.4	-0.40
3839.639	30008.894	ev	3.5	3972.167	od	4.5	25.8 ± 1.4	-0.34
3842.205	35111.830	od	6.5	9092.491	ev	5.5	57.7 ± 3.0	0.25
3843.800	30849.648	ev	4.5	4841.106	od	5.5	2.13 ± 0.14	-1.33
3844.578	27162.224	ev	4.5	1158.943	od	5.5	15.7 ± 0.8	-0.46
3850.699	26595.222	ev	3.5	633.273	od	4.5	33.9 ± 1.7	-0.22
3850.977	25960.073	ev	1.5	0.000	od	2.5	107 ± 5	-0.02
3852.461	26211.912	ev	2.5	261.841	od	3.5	60 ± 3	-0.10
3854.167	29965.752	ev	2.5	4027.161	od	1.5	4.29 ± 0.29	-1.24
3855.559	27864.534	ev	5.5	1935.310	od	6.5	4.37 ± 0.28	-0.93
3867.259	29877.937	ev	1.5	4027.161	od	1.5	8.5 ± 0.5	-1.12
3871.543	26455.446	ev	4.5	633.273	od	4.5	1.51 ± 0.09	-1.47
3872.623	29242.250	ev	3.5	3427.274	od	3.5	2.76 ± 0.20	-1.30
3875.451	30008.894	ev	3.5	4212.756	od	2.5	4.47 ± 0.29	-1.09
3881.844	29197.887	ev	2.5	3444.235	od	3.5	2.27 ± 0.24	-1.51
3881.943	29965.752	ev	2.5	4212.756	od	2.5	1.62 ± 0.14	-1.66
3887.151	26351.767	ev	4.5	633.273	od	4.5	0.65 ± 0.05	-1.83
3890.846	36778.403	od	4.5	11084.335	ev	3.5	4.5 ± 0.4	-0.99
3894.693	25668.692	ev	3.5	0.000	od	2.5	14.3 ± 0.7	-0.58
3895.226	29877.937	ev	1.5	4212.756	od	2.5	9.3 ± 0.6	-1.07
3895.786	35605.266	od	5.5	9943.779	ev	5.5	25.8 ± 1.3	-0.15
3896.411	30996.851	ev	6.5	5339.477	od	5.5	0.74 ± 0.11	-1.63
3902.397	29045.291	ev	4.5	3427.274	od	3.5	11.6 ± 0.7	-0.58
3913.778	30027.378	ev	4.5	4483.854	od	3.5	1.02 ± 0.11	-1.63
3916.509	30366.818	ev	5.5	4841.106	od	5.5	32.7 ± 2.3	-0.04
3916.612	30008.894	ev	3.5	4483.854	od	3.5	0.54 ± 0.08	-2.00
3918.057	34608.122	od	5.5	9092.491	ev	5.5	5.7 ± 0.4	-0.80

Table 3—Continued

λ_{air} (Å)	E_{upper} (cm^{-1})	Parity	J_{upp}	E_{lower} (cm^{-1})	Parity	J_{low}	A-value (10^6 s^{-1})	$\text{Log}(gf)$
3918.228	30366.818	ev	5.5	4852.304	od	4.5	1.87 ± 0.15	-1.29
3923.243	29965.752	ev	2.5	4483.854	od	3.5	9.4 ± 0.6	-0.89
3930.496	36778.403	od	4.5	11343.525	ev	4.5	1.43 ± 0.14	-1.48
3932.975	35362.630	od	6.5	9943.779	ev	5.5	4.88 ± 0.29	-0.80
3934.832	25668.692	ev	3.5	261.841	od	3.5	4.97 ± 0.26	-1.04
3938.969	36723.695	od	5.5	11343.525	ev	4.5	7.6 ± 0.4	-0.68
3951.997	26455.446	ev	4.5	1158.943	od	5.5	2.53 ± 0.14	-1.23
3956.129	29242.250	ev	3.5	3972.167	od	4.5	0.45 ± 0.06	-2.08
3957.667	30101.366	ev	5.5	4841.106	od	5.5	20.2 ± 1.2	-0.25
3959.423	30101.366	ev	5.5	4852.304	od	4.5	5.2 ± 0.4	-0.84
3959.529	31145.651	ev	7.5	5897.264	od	6.5	5.1 ± 0.4	-0.71
3966.857	28629.017	ev	2.5	3427.274	od	3.5	0.98 ± 0.16	-1.86
3968.262	26351.767	ev	4.5	1158.943	od	5.5	0.97 ± 0.06	-1.64
3969.294	30027.378	ev	4.5	4841.106	od	5.5	5.8 ± 0.5	-0.86
3971.060	30027.378	ev	4.5	4852.304	od	4.5	2.7 ± 0.4	-1.19
3971.745	29197.887	ev	2.5	4027.161	od	1.5	13.0 ± 0.8	-0.73
3972.168	35111.830	od	6.5	9943.779	ev	5.5	4.7 ± 0.3	-0.81
3973.977	30008.894	ev	3.5	4852.304	od	4.5	14.1 ± 0.8	-0.57
3983.003	30996.851	ev	6.5	5897.264	od	6.5	2.83 ± 0.25	-1.03
3987.207	29045.291	ev	4.5	3972.167	od	4.5	7.3 ± 0.5	-0.76
3991.688	33596.027	ev	4.5	8551.049	od	5.5	2.5 ± 0.5	-1.23
3993.212	25668.692	ev	3.5	633.273	od	4.5	2.01 ± 0.12	-1.41
3994.157	29242.250	ev	3.5	4212.756	od	2.5	9.8 ± 0.7	-0.73
3996.314	34108.475	od	4.5	9092.491	ev	5.5	34.1 ± 1.8	-0.09
3997.766	33557.951	ev	6.5	8551.049	od	5.5	8.8 ± 0.7	-0.53
4001.249	29197.887	ev	2.5	4212.756	od	2.5	11.5 ± 0.8	-0.78
4003.842	36461.156	ev	5.5	11492.204	od	5.5	4.6 ± 0.4	-0.87
4013.952	27988.074	ev	3.5	3082.011	od	2.5	1.46 ± 0.14	-1.55
4037.323	30101.366	ev	5.5	5339.477	od	5.5	26.5 ± 1.6	-0.11
4037.893	29242.250	ev	3.5	4483.854	od	3.5	19.4 ± 1.3	-0.42
4045.141	29197.887	ev	2.5	4483.854	od	3.5	5.4 ± 0.4	-1.10

Table 3—Continued

λ_{air} (Å)	E_{upper} (cm^{-1})	Parity	J_{upp}	E_{lower} (cm^{-1})	Parity	J_{low}	A-value (10^6 s^{-1})	$\text{Log}(gf)$
4049.423	30027.378	ev	4.5	5339.477	od	5.5	33.5 ± 2.4	-0.08
4049.854	32677.540	od	6.5	7992.268	ev	6.5	89 ± 4	0.49
4053.291	34608.122	od	5.5	9943.779	ev	5.5	56.1 ± 2.9	0.22
4062.587	34900.473	od	3.5	10292.567	ev	4.5	57.3 ± 2.9	0.06
4063.384	32595.348	od	5.5	7992.268	ev	6.5	72 ± 4	0.33
4063.586	28629.017	ev	2.5	4027.161	od	1.5	11.5 ± 0.9	-0.77
4070.274	29045.291	ev	4.5	4483.854	od	3.5	12.2 ± 0.8	-0.52
4070.379	27988.074	ev	3.5	3427.274	od	3.5	4.41 ± 0.28	-1.06
4073.192	27988.074	ev	3.5	3444.235	od	3.5	7.0 ± 0.4	-0.86
4073.747	31145.651	ev	7.5	6605.154	od	7.5	27.8 ± 2.0	0.04
4075.466	28502.312	ev	5.5	3972.167	od	4.5	0.48 ± 0.07	-1.84
4078.443	29353.344	ev	6.5	4841.106	od	5.5	16.9 ± 1.1	-0.23
4085.558	30366.818	ev	5.5	5897.264	od	6.5	33.0 ± 2.5	0.00
4087.134	36778.403	od	4.5	12318.288	ev	3.5	1.00 ± 0.17	-1.60
4094.475	28629.017	ev	2.5	4212.756	od	2.5	9.3 ± 0.7	-0.85
4098.019	32946.196	ev	5.5	8551.049	od	5.5	1.72 ± 0.17	-1.28
4098.599	30996.851	ev	6.5	6605.154	od	7.5	67 ± 5	0.37
4098.893	29242.250	ev	3.5	4852.304	od	4.5	16.5 ± 1.1	-0.48
4111.434	34608.122	od	5.5	10292.567	ev	4.5	19.9 ± 1.1	-0.22
4120.553	35605.266	od	5.5	11343.525	ev	4.5	0.66 ± 0.05	-1.70
4128.383	27297.741	ev	2.5	3082.011	od	2.5	0.48 ± 0.04	-2.14
4132.264	29045.291	ev	4.5	4852.304	od	4.5	27.6 ± 1.8	-0.15
4137.102	34108.475	od	4.5	9943.779	ev	5.5	29.8 ± 1.6	-0.12
4140.449	28629.017	ev	2.5	4483.854	od	3.5	3.88 ± 0.28	-1.22
4154.865	32946.196	ev	5.5	8884.809	od	4.5	7.3 ± 0.6	-0.65
4162.733	27988.074	ev	3.5	3972.167	od	4.5	8.9 ± 0.6	-0.73
4184.258	27864.534	ev	5.5	3972.167	od	4.5	31.4 ± 1.8	0.00
4188.097	27297.741	ev	2.5	3427.274	od	3.5	2.06 ± 0.14	-1.49
4191.075	27297.741	ev	2.5	3444.235	od	3.5	20.9 ± 1.3	-0.48
4197.651	34900.473	od	3.5	11084.335	ev	3.5	13.7 ± 0.9	-0.54
4197.691	34108.475	od	4.5	10292.567	ev	4.5	22.3 ± 1.2	-0.23

Table 3—Continued

λ_{air} (Å)	E_{upper} (cm^{-1})	Parity	J_{upp}	E_{lower} (cm^{-1})	Parity	J_{low}	A-value (10^6 s^{-1})	Log(gf)
4204.858	27988.074	ev	3.5	4212.756	od	2.5	10.6 ± 0.7	-0.65
4208.745	32304.409	ev	4.5	8551.049	od	5.5	0.63 ± 0.06	-1.78
4215.022	27162.224	ev	4.5	3444.235	od	3.5	13.8 ± 0.9	-0.44
4217.187	29045.291	ev	4.5	5339.477	od	5.5	15.4 ± 1.1	-0.39
4225.137	28502.312	ev	5.5	4841.106	od	5.5	3.37 ± 0.23	-0.97
4227.138	28502.312	ev	5.5	4852.304	od	4.5	3.71 ± 0.25	-0.92
4235.072	32490.510	ev	3.5	8884.809	od	4.5	1.34 ± 0.12	-1.54
4238.781	32677.540	od	6.5	9092.491	ev	5.5	16.8 ± 0.9	-0.20
4243.837	34900.473	od	3.5	11343.525	ev	4.5	16.6 ± 1.0	-0.44
4246.567	32684.712	ev	4.5	9142.904	od	3.5	8.6 ± 0.7	-0.63
4251.731	26595.222	ev	3.5	3082.011	od	2.5	27.8 ± 1.6	-0.22
4253.358	27988.074	ev	3.5	4483.854	od	3.5	14.1 ± 1.0	-0.52
4253.604	32595.348	od	5.5	9092.491	ev	5.5	27.7 ± 1.5	-0.04
4268.726	32304.409	ev	4.5	8884.809	od	4.5	8.6 ± 0.8	-0.63
4275.023	36461.156	ev	5.5	13076.050	od	4.5	0.89 ± 0.09	-1.53
4280.491	26211.912	ev	2.5	2856.678	od	1.5	19.2 ± 1.1	-0.50
4296.063	27297.741	ev	2.5	4027.161	od	1.5	17.3 ± 1.1	-0.54
4297.168	34608.122	od	5.5	11343.525	ev	4.5	19.1 ± 1.1	-0.20
4303.455	34900.473	od	3.5	11669.863	ev	2.5	2.21 ± 0.13	-1.31
4310.980	27162.224	ev	4.5	3972.167	od	4.5	2.07 ± 0.14	-1.24
4316.047	28502.312	ev	5.5	5339.477	od	5.5	10.6 ± 0.7	-0.45
4316.269	32490.510	ev	3.5	9328.864	od	2.5	7.7 ± 0.6	-0.77
4321.096	27988.074	ev	3.5	4852.304	od	4.5	5.4 ± 0.5	-0.91
4322.193	26211.912	ev	2.5	3082.011	od	2.5	2.59 ± 0.16	-1.36
4324.065	32262.787	ev	3.5	9142.904	od	3.5	9.0 ± 0.8	-0.69
4324.564	32260.120	ev	2.5	9142.904	od	3.5	3.06 ± 0.26	-1.29
4325.557	34178.776	ev	5.5	11066.865	od	4.5	16.9 ± 2.4	-0.25
4327.151	25960.073	ev	1.5	2856.678	od	1.5	18.4 ± 1.1	-0.69
4330.602	27297.741	ev	2.5	4212.756	od	2.5	11.1 ± 0.7	-0.73
4330.941	36461.156	ev	5.5	13377.976	od	5.5	4.4 ± 0.4	-0.83
4341.287	26455.446	ev	4.5	3427.274	od	3.5	7.1 ± 0.4	-0.70

Table 3—Continued

λ_{air} (Å)	E_{upper} (cm^{-1})	Parity	J_{upp}	E_{lower} (cm^{-1})	Parity	J_{low}	A-value (10^6 s^{-1})	$\text{Log}(gf)$
4342.181	27864.534	ev	5.5	4841.106	od	5.5	15.9 ± 1.1	-0.27
4344.294	27864.534	ev	5.5	4852.304	od	4.5	2.49 ± 0.18	-1.07
4344.486	26455.446	ev	4.5	3444.235	od	3.5	0.66 ± 0.05	-1.73
4347.307	33596.027	ev	4.5	10599.743	od	3.5	21.9 ± 3.0	-0.21
4359.635	32260.120	ev	2.5	9328.864	od	2.5	2.57 ± 0.27	-1.36
4360.921	26351.767	ev	4.5	3427.274	od	3.5	2.75 ± 0.14	-1.11
4364.150	26351.767	ev	4.5	3444.235	od	3.5	0.335 ± 0.022	-2.02
4369.772	25960.073	ev	1.5	3082.011	od	2.5	14.3 ± 1.1	-0.79
4374.252	32946.196	ev	5.5	10091.567	od	4.5	1.70 ± 0.20	-1.23
4380.644	32150.143	ev	2.5	9328.864	od	2.5	10.9 ± 1.0	-0.72
4382.064	27297.741	ev	2.5	4483.854	od	3.5	2.78 ± 0.19	-1.32
4383.114	32260.120	ev	2.5	9451.697	od	1.5	13.6 ± 1.1	-0.63
4387.689	26211.912	ev	2.5	3427.274	od	3.5	6.5 ± 0.4	-0.95
4390.958	26211.912	ev	2.5	3444.235	od	3.5	5.2 ± 0.3	-1.04
4391.432	31908.123	ev	3.5	9142.904	od	3.5	5.7 ± 0.5	-0.88
4391.484	34108.475	od	4.5	11343.525	ev	4.5	2.61 ± 0.20	-1.12
4394.720	29353.344	ev	6.5	6605.154	od	7.5	0.74 ± 0.07	-1.53
4397.509	32677.540	od	6.5	9943.779	ev	5.5	10.6 ± 0.6	-0.36
4400.178	32048.837	ev	1.5	9328.864	od	2.5	3.6 ± 0.3	-1.37
4406.656	34178.776	ev	5.5	11492.204	od	5.5	25 ± 3	-0.05
4408.250	27162.224	ev	4.5	4483.854	od	3.5	6.1 ± 0.4	-0.75
4413.466	32595.348	od	5.5	9943.779	ev	5.5	1.08 ± 0.10	-1.42
4419.029	26595.222	ev	3.5	3972.167	od	4.5	8.5 ± 0.5	-0.70
4421.240	33211.481	ev	3.5	10599.743	od	3.5	18.7 ± 2.9	-0.36
4424.096	32048.837	ev	1.5	9451.697	od	1.5	5.7 ± 0.6	-1.17
4426.145	25668.692	ev	3.5	3082.011	od	2.5	1.12 ± 0.08	-1.58
4427.026	34900.473	od	3.5	12318.288	ev	3.5	3.19 ± 0.29	-1.12
4427.600	31908.123	ev	3.5	9328.864	od	2.5	3.8 ± 0.4	-1.04
4437.446	33596.027	ev	4.5	11066.865	od	4.5	1.21 ± 0.20	-1.45
4438.254	27864.534	ev	5.5	5339.477	od	5.5	4.3 ± 0.3	-0.82
4446.502	26455.446	ev	4.5	3972.167	od	4.5	1.75 ± 0.12	-1.28

Table 3—Continued

λ_{air} (Å)	E_{upper} (cm^{-1})	Parity	J_{upp}	E_{lower} (cm^{-1})	Parity	J_{low}	A-value (10^6 s^{-1})	$\text{Log}(gf)$
4453.926	30996.851	ev	6.5	8551.049	od	5.5	1.17 ± 0.12	-1.31
4463.244	32490.510	ev	3.5	10091.567	od	4.5	4.6 ± 0.5	-0.95
4466.529	26595.222	ev	3.5	4212.756	od	2.5	6.4 ± 0.4	-0.82
4478.806	27162.224	ev	4.5	4841.106	od	5.5	5.0 ± 0.4	-0.82
4481.054	27162.224	ev	4.5	4852.304	od	4.5	6.0 ± 0.4	-0.74
4482.488	32595.348	od	5.5	10292.567	ev	4.5	0.284 ± 0.028	-1.99
4483.329	30849.648	ev	4.5	8551.049	od	5.5	12.7 ± 0.9	-0.42
4484.470	32684.712	ev	4.5	10391.789	od	3.5	1.30 ± 0.15	-1.41
4494.855	25668.692	ev	3.5	3427.274	od	3.5	0.299 ± 0.019	-2.14
4498.286	25668.692	ev	3.5	3444.235	od	3.5	3.41 ± 0.23	-1.08
4500.638	32304.409	ev	4.5	10091.567	od	4.5	0.85 ± 0.09	-1.59
4506.337	26211.912	ev	2.5	4027.161	od	1.5	5.1 ± 0.4	-1.03
4509.087	32262.787	ev	3.5	10091.567	od	4.5	3.1 ± 0.3	-1.13
4514.504	33211.481	ev	3.5	11066.865	od	4.5	23 ± 3	-0.25
4521.293	26595.222	ev	3.5	4483.854	od	3.5	1.32 ± 0.11	-1.49
4522.836	33596.027	ev	4.5	11492.204	od	5.5	15.9 ± 2.3	-0.31
4523.880	32490.510	ev	3.5	10391.789	od	3.5	1.37 ± 0.14	-1.47
4530.640	33557.951	ev	6.5	11492.204	od	5.5	0.34 ± 0.04	-1.83
4550.056	26455.446	ev	4.5	4483.854	od	3.5	0.078 ± 0.010	-2.62
4550.951	27864.534	ev	5.5	5897.264	od	6.5	1.32 ± 0.10	-1.31
4551.455	30849.648	ev	4.5	8884.809	od	4.5	1.01 ± 0.09	-1.50
4558.080	25960.073	ev	1.5	4027.161	od	1.5	5.2 ± 0.4	-1.19
4566.856	32490.510	ev	3.5	10599.743	od	3.5	0.25 ± 0.04	-2.20
4570.984	32262.787	ev	3.5	10391.789	od	3.5	1.71 ± 0.17	-1.37
4571.629	26351.767	ev	4.5	4483.854	od	3.5	0.039 ± 0.005	-2.92
4581.091	27162.224	ev	4.5	5339.477	od	5.5	1.85 ± 0.17	-1.23
4582.391	31908.123	ev	3.5	10091.567	od	4.5	9.6 ± 0.9	-0.62
4582.556	30366.818	ev	5.5	8551.049	od	5.5	7.0 ± 0.8	-0.57
4587.936	34108.475	od	4.5	12318.288	ev	3.5	0.24 ± 0.03	-2.13
4596.980	25960.073	ev	1.5	4212.756	od	2.5	7.9 ± 0.7	-1.00
4597.910	26595.222	ev	3.5	4852.304	od	4.5	5.9 ± 0.4	-0.83

Table 3—Continued

λ_{air} (Å)	E_{upper} (cm^{-1})	Parity	J_{upp}	E_{lower} (cm^{-1})	Parity	J_{low}	A-value (10^6 s^{-1})	$\text{Log}(gf)$
4601.055	26211.912	ev	2.5	4483.854	od	3.5	8.2 ± 0.6	-0.81
4605.573	30849.648	ev	4.5	9142.904	od	3.5	0.232 ± 0.026	-2.13
4622.547	32260.120	ev	2.5	10633.083	od	2.5	0.31 ± 0.05	-2.22
4625.263	26455.446	ev	4.5	4841.106	od	5.5	0.043 ± 0.005	-2.86
4627.660	26455.446	ev	4.5	4852.304	od	4.5	0.38 ± 0.03	-1.92
4639.004	30101.366	ev	5.5	8551.049	od	5.5	2.86 ± 0.26	-0.96
4646.331	31908.123	ev	3.5	10391.789	od	3.5	2.45 ± 0.25	-1.20
4649.977	26351.767	ev	4.5	4852.304	od	4.5	0.162 ± 0.012	-2.28
4653.755	30366.818	ev	5.5	8884.809	od	4.5	0.35 ± 0.05	-1.86
4654.986	30027.378	ev	4.5	8551.049	od	5.5	2.37 ± 0.27	-1.11
4659.071	32260.120	ev	2.5	10802.621	od	1.5	0.49 ± 0.11	-2.01
4659.410	25668.692	ev	3.5	4212.756	od	2.5	0.277 ± 0.024	-2.14
4659.833	32946.196	ev	5.5	11492.204	od	5.5	0.74 ± 0.09	-1.54
4666.433	32490.510	ev	3.5	11066.865	od	4.5	1.91 ± 0.20	-1.30
4691.676	31908.123	ev	3.5	10599.743	od	3.5	0.41 ± 0.06	-1.97
4707.325	32304.409	ev	4.5	11066.865	od	4.5	0.52 ± 0.08	-1.76
4711.982	30101.366	ev	5.5	8884.809	od	4.5	1.49 ± 0.14	-1.23
4716.569	32262.787	ev	3.5	11066.865	od	4.5	1.37 ± 0.15	-1.44
4719.037	25668.692	ev	3.5	4483.854	od	3.5	0.50 ± 0.04	-1.87
4728.471	30027.378	ev	4.5	8884.809	od	4.5	5.7 ± 0.6	-0.72
4732.609	30008.894	ev	3.5	8884.809	od	4.5	10.6 ± 1.0	-0.54
4734.428	26455.446	ev	4.5	5339.477	od	5.5	0.88 ± 0.09	-1.53
4757.789	26351.767	ev	4.5	5339.477	od	5.5	0.35 ± 0.03	-1.92
4786.908	30027.378	ev	4.5	9142.904	od	3.5	2.4 ± 0.3	-1.09
4791.148	30008.894	ev	3.5	9142.904	od	3.5	0.97 ± 0.08	-1.57
4801.075	29965.752	ev	2.5	9142.904	od	3.5	10.0 ± 1.0	-0.68
4802.565	25668.692	ev	3.5	4852.304	od	4.5	0.48 ± 0.05	-1.87
4803.530	32304.409	ev	4.5	11492.204	od	5.5	1.90 ± 0.27	-1.18
4805.819	29353.344	ev	6.5	8551.049	od	5.5	0.79 ± 0.09	-1.42
4806.164	34178.776	ev	5.5	13377.976	od	5.5	1.6 ± 0.3	-1.17
4834.232	30008.894	ev	3.5	9328.864	od	2.5	3.5 ± 0.3	-1.00

Table 3—Continued

λ_{air} (Å)	E_{upper} (cm^{-1})	Parity	J_{upp}	E_{lower} (cm^{-1})	Parity	J_{low}	A-value (10^6 s^{-1})	$\text{Log}(gf)$
4865.041	29877.937	ev	1.5	9328.864	od	2.5	9.6 ± 0.9	-0.87
4871.939	33596.027	ev	4.5	13076.050	od	4.5	0.86 ± 0.19	-1.51
4873.345	29965.752	ev	2.5	9451.697	od	1.5	2.42 ± 0.26	-1.29
4878.057	29045.291	ev	4.5	8551.049	od	5.5	0.40 ± 0.07	-1.85
4894.297	29877.937	ev	1.5	9451.697	od	1.5	5.2 ± 0.5	-1.12
4910.838	29242.250	ev	3.5	8884.809	od	4.5	0.80 ± 0.13	-1.64
4936.152	34178.776	ev	5.5	13925.734	od	6.5	3.2 ± 0.7	-0.86
4936.917	30849.648	ev	4.5	10599.743	od	3.5	0.42 ± 0.05	-1.82
4944.695	33596.027	ev	4.5	13377.976	od	5.5	1.8 ± 0.4	-1.18
4958.815	29045.291	ev	4.5	8884.809	od	4.5	1.13 ± 0.18	-1.38
4973.898	29242.250	ev	3.5	9142.904	od	3.5	0.70 ± 0.10	-1.68
4984.901	29197.887	ev	2.5	9142.904	od	3.5	0.90 ± 0.10	-1.70
5010.816	28502.312	ev	5.5	8551.049	od	5.5	1.65 ± 0.21	-1.13
5019.354	30008.894	ev	3.5	10091.567	od	4.5	1.48 ± 0.15	-1.35
5023.122	29045.291	ev	4.5	9142.904	od	3.5	1.49 ± 0.19	-1.25
5031.273	32946.196	ev	5.5	13076.050	od	4.5	3.2 ± 0.4	-0.84
5031.557	29197.887	ev	2.5	9328.864	od	2.5	1.54 ± 0.18	-1.45
5050.878	32684.712	ev	4.5	12891.692	od	3.5	4.4 ± 0.6	-0.77
5062.857	29197.887	ev	2.5	9451.697	od	1.5	1.33 ± 0.16	-1.51
5071.010	32490.510	ev	3.5	12776.067	od	2.5	3.2 ± 0.5	-1.00
5092.249	33557.951	ev	6.5	13925.734	od	6.5	10.9 ± 1.3	-0.23
5096.068	28502.312	ev	5.5	8884.809	od	4.5	1.21 ± 0.16	-1.25
5098.366	32684.712	ev	4.5	13076.050	od	4.5	6.0 ± 0.8	-0.63
5100.927	32490.510	ev	3.5	12891.692	od	3.5	2.6 ± 0.4	-1.10
5107.404	29965.752	ev	2.5	10391.789	od	3.5	1.05 ± 0.15	-1.61
5108.903	32946.196	ev	5.5	13377.976	od	5.5	9.3 ± 1.1	-0.36
5111.920	32260.120	ev	2.5	12703.450	od	1.5	1.17 ± 0.17	-1.56
5125.555	30996.851	ev	6.5	11492.204	od	5.5	3.2 ± 0.5	-0.75
5130.270	32262.787	ev	3.5	12776.067	od	2.5	3.7 ± 0.5	-0.93
5140.830	32150.143	ev	2.5	12703.450	od	1.5	6.0 ± 1.0	-0.84
5149.365	32490.510	ev	3.5	13076.050	od	4.5	0.77 ± 0.11	-1.61

Table 3—Continued

λ_{air} (Å)	E_{upper} (cm^{-1})	Parity	J_{upp}	E_{lower} (cm^{-1})	Parity	J_{low}	A-value (10^6 s^{-1})	$\text{Log}(gf)$
5149.828	32304.409	ev	4.5	12891.692	od	3.5	1.01 ± 0.19	-1.40
5156.752	32048.837	ev	1.5	12662.186	od	0.5	6.6 ± 0.9	-0.98
5160.099	32150.143	ev	2.5	12776.067	od	2.5	1.23 ± 0.15	-1.53
5160.893	32262.787	ev	3.5	12891.692	od	3.5	2.15 ± 0.26	-1.16
5161.604	32260.120	ev	2.5	12891.692	od	3.5	0.94 ± 0.19	-1.65
5176.288	27864.534	ev	5.5	8551.049	od	5.5	3.8 ± 0.5	-0.74
5178.097	32684.712	ev	4.5	13377.976	od	5.5	1.65 ± 0.26	-1.18
5179.917	30366.818	ev	5.5	11066.865	od	4.5	1.04 ± 0.20	-1.30
5187.223	32048.837	ev	1.5	12776.067	od	2.5	7.9 ± 1.1	-0.90
5191.080	32150.143	ev	2.5	12891.692	od	3.5	4.7 ± 0.7	-0.94
5199.204	32304.409	ev	4.5	13076.050	od	4.5	1.27 ± 0.19	-1.29
5210.483	32262.787	ev	3.5	13076.050	od	4.5	3.3 ± 0.4	-0.97
5213.041	28629.017	ev	2.5	9451.697	od	1.5	0.18 ± 0.04	-2.35
5220.292	29242.250	ev	3.5	10091.567	od	4.5	2.30 ± 0.30	-1.12
5256.033	32946.196	ev	5.5	13925.734	od	6.5	1.10 ± 0.16	-1.26
5267.314	27864.534	ev	5.5	8884.809	od	4.5	0.172 ± 0.021	-2.07
5272.652	30027.378	ev	4.5	11066.865	od	4.5	0.37 ± 0.08	-1.81
5282.146	32304.409	ev	4.5	13377.976	od	5.5	0.50 ± 0.08	-1.68
5303.434	29242.250	ev	3.5	10391.789	od	3.5	0.40 ± 0.05	-1.87
5304.923	27988.074	ev	3.5	9142.904	od	3.5	0.24 ± 0.03	-2.09
5357.794	27988.074	ev	3.5	9328.864	od	2.5	0.61 ± 0.08	-1.68
5362.155	36461.156	ev	5.5	17817.123	od	4.5	1.52 ± 0.24	-1.10
5362.594	29242.250	ev	3.5	10599.743	od	3.5	0.35 ± 0.07	-1.92
5371.622	27162.224	ev	4.5	8551.049	od	5.5	0.247 ± 0.028	-1.97
5375.386	29197.887	ev	2.5	10599.743	od	3.5	1.29 ± 0.21	-1.48
5393.648	30027.378	ev	4.5	11492.204	od	5.5	0.71 ± 0.12	-1.51
5417.091	36821.816	od	6.5	18366.854	ev	7.5	1.28 ± 0.19	-1.10
5419.856	29045.291	ev	4.5	10599.743	od	3.5	0.83 ± 0.11	-1.43
5423.635	36821.816	od	6.5	18389.122	ev	6.5	1.45 ± 0.20	-1.05
5452.661	36723.695	od	5.5	18389.122	ev	6.5	1.77 ± 0.23	-1.02
5500.419	29242.250	ev	3.5	11066.865	od	4.5	1.64 ± 0.21	-1.23

Table 3—Continued

λ_{air} (Å)	E_{upper} (cm^{-1})	Parity	J_{upp}	E_{lower} (cm^{-1})	Parity	J_{low}	A-value (10^6 s^{-1})	$\text{Log}(gf)$
5510.566	36461.156	ev	5.5	18319.239	od	4.5	0.75 ± 0.13	-1.38
5513.665	36821.816	od	6.5	18690.096	ev	5.5	0.82 ± 0.12	-1.28
5544.995	28629.017	ev	2.5	10599.743	od	3.5	0.87 ± 0.11	-1.62
5555.268	28629.017	ev	2.5	10633.083	od	2.5	0.121 ± 0.018	-2.47
5560.678	29045.291	ev	4.5	11066.865	od	4.5	1.76 ± 0.24	-1.09
5583.670	26455.446	ev	4.5	8551.049	od	5.5	1.23 ± 0.15	-1.24
5597.193	29353.344	ev	6.5	11492.204	od	5.5	0.45 ± 0.05	-1.52
5616.192	26351.767	ev	4.5	8551.049	od	5.5	0.55 ± 0.06	-1.58
5621.411	36461.156	ev	5.5	18676.965	od	6.5	2.17 ± 0.26	-0.91
5624.761	30849.648	ev	4.5	13076.050	od	4.5	0.155 ± 0.019	-2.13
5644.829	26595.222	ev	3.5	8884.809	od	4.5	0.66 ± 0.08	-1.60
5721.963	30849.648	ev	4.5	13377.976	od	5.5	1.18 ± 0.14	-1.24
5728.309	26595.222	ev	3.5	9142.904	od	3.5	0.226 ± 0.025	-2.05
5733.852	28502.312	ev	5.5	11066.865	od	4.5	3.6 ± 0.5	-0.67
5749.389	27988.074	ev	3.5	10599.743	od	3.5	1.37 ± 0.19	-1.27
5763.188	36723.695	od	5.5	19376.999	ev	4.5	0.28 ± 0.03	-1.77
5774.558	26455.446	ev	4.5	9142.904	od	3.5	0.088 ± 0.017	-2.35
5790.004	26595.222	ev	3.5	9328.864	od	2.5	0.192 ± 0.026	-2.11
5801.270	30008.894	ev	3.5	12776.067	od	2.5	0.55 ± 0.06	-1.66
5807.024	29877.937	ev	1.5	12662.186	od	0.5	3.2 ± 0.5	-1.19
5815.830	29965.752	ev	2.5	12776.067	od	2.5	2.9 ± 0.4	-1.05
5820.976	29877.937	ev	1.5	12703.450	od	1.5	4.3 ± 0.5	-1.06
5840.457	30008.894	ev	3.5	12891.692	od	3.5	2.6 ± 0.4	-0.97
5845.693	29877.937	ev	1.5	12776.067	od	2.5	2.5 ± 0.4	-1.29
5855.215	29965.752	ev	2.5	12891.692	od	3.5	3.1 ± 0.4	-1.02
5856.948	26211.912	ev	2.5	9142.904	od	3.5	0.72 ± 0.08	-1.65
5877.229	28502.312	ev	5.5	11492.204	od	5.5	1.76 ± 0.23	-0.96
5882.185	35362.630	od	6.5	18366.854	ev	7.5	1.60 ± 0.19	-0.94
5889.902	35362.630	od	6.5	18389.122	ev	6.5	0.47 ± 0.06	-1.47
5904.046	30008.894	ev	3.5	13076.050	od	4.5	4.7 ± 0.6	-0.71
5913.529	35272.546	od	7.5	18366.854	ev	7.5	7.4 ± 0.9	-0.21

Table 3—Continued

λ_{air} (Å)	E_{upper} (cm^{-1})	Parity	J_{upp}	E_{lower} (cm^{-1})	Parity	J_{low}	A-value (10^6 s^{-1})	Log(gf)
5921.328	35272.546	od	7.5	18389.122	ev	6.5	1.53 ± 0.21	-0.89
5951.558	27864.534	ev	5.5	11066.865	od	4.5	0.26 ± 0.04	-1.78
5956.447	25668.692	ev	3.5	8884.809	od	4.5	0.63 ± 0.08	-1.57
5964.858	26211.912	ev	2.5	9451.697	od	1.5	0.149 ± 0.018	-2.32
5970.287	35111.830	od	6.5	18366.854	ev	7.5	2.3 ± 0.3	-0.77
5976.141	36821.816	od	6.5	20093.245	ev	5.5	0.68 ± 0.09	-1.29
5978.237	35111.830	od	6.5	18389.122	ev	6.5	0.31 ± 0.05	-1.64
5982.409	36461.156	ev	5.5	19750.111	od	5.5	2.7 ± 0.4	-0.75
5987.084	27297.741	ev	2.5	10599.743	od	3.5	1.03 ± 0.16	-1.48
5996.228	35362.630	od	6.5	18690.096	ev	5.5	0.23 ± 0.03	-1.77
6004.559	30027.378	ev	4.5	13377.976	od	5.5	3.1 ± 0.5	-0.78
6011.127	25960.073	ev	1.5	9328.864	od	2.5	0.49 ± 0.06	-1.97
6036.071	27162.224	ev	4.5	10599.743	od	3.5	0.082 ± 0.012	-2.35
6049.474	25668.692	ev	3.5	9142.904	od	3.5	0.191 ± 0.022	-2.08
6053.652	36461.156	ev	5.5	19946.775	od	4.5	0.26 ± 0.05	-1.77
6055.854	25960.073	ev	1.5	9451.697	od	1.5	0.194 ± 0.026	-2.37
6080.641	30366.818	ev	5.5	13925.734	od	6.5	2.1 ± 0.4	-0.85
6106.176	27864.534	ev	5.5	11492.204	od	5.5	0.50 ± 0.08	-1.47
6180.428	30101.366	ev	5.5	13925.734	od	6.5	1.79 ± 0.28	-0.91
6190.417	36723.695	od	5.5	20574.163	ev	4.5	0.29 ± 0.05	-1.70
6260.307	29045.291	ev	4.5	13076.050	od	4.5	0.42 ± 0.08	-1.60
6280.449	34608.122	od	5.5	18690.096	ev	5.5	0.35 ± 0.04	-1.61
6305.135	26455.446	ev	4.5	10599.743	od	3.5	1.44 ± 0.19	-1.07
6314.217	33557.951	ev	6.5	17725.052	od	5.5	0.88 ± 0.13	-1.13
6346.636	26351.767	ev	4.5	10599.743	od	3.5	0.44 ± 0.05	-1.57
6380.951	29045.291	ev	4.5	13377.976	od	5.5	1.13 ± 0.15	-1.16
6382.171	36821.816	od	6.5	21157.496	ev	6.5	3.0 ± 0.4	-0.59
6422.401	36723.695	od	5.5	21157.496	ev	6.5	3.2 ± 0.5	-0.62
6434.297	34178.776	ev	5.5	18641.357	od	5.5	0.28 ± 0.06	-1.68
6440.077	34900.473	od	3.5	19376.999	ev	4.5	0.38 ± 0.04	-1.73
6444.832	35605.266	od	5.5	20093.245	ev	5.5	0.97 ± 0.12	-1.14

Table 3—Continued

λ_{air} (Å)	E_{upper} (cm^{-1})	Parity	J_{upp}	E_{lower} (cm^{-1})	Parity	J_{low}	A-value (10^6 s^{-1})	$\text{Log}(gf)$
6480.095	29353.344	ev	6.5	13925.734	od	6.5	0.47 ± 0.08	-1.38
6483.974	34108.475	od	4.5	18690.096	ev	5.5	0.72 ± 0.09	-1.34
6494.092	33211.481	ev	3.5	17817.123	od	4.5	0.89 ± 0.18	-1.34
6547.244	35362.630	od	6.5	20093.245	ev	5.5	0.33 ± 0.04	-1.53
6563.691	34608.122	od	5.5	19376.999	ev	4.5	0.63 ± 0.08	-1.31
6567.994	32946.196	ev	5.5	17725.052	od	5.5	0.84 ± 0.13	-1.18
6622.275	27988.074	ev	3.5	12891.692	od	3.5	0.24 ± 0.03	-1.90
6634.331	25668.692	ev	3.5	10599.743	od	3.5	1.25 ± 0.15	-1.18
6651.035	35605.266	od	5.5	20574.163	ev	4.5	0.34 ± 0.05	-1.56
6656.579	35111.830	od	6.5	20093.245	ev	5.5	0.42 ± 0.05	-1.41
6681.199	26455.446	ev	4.5	11492.204	od	5.5	0.97 ± 0.12	-1.19
6702.093	33557.951	ev	6.5	18641.357	od	5.5	0.76 ± 0.14	-1.15
6704.147	27988.074	ev	3.5	13076.050	od	4.5	0.36 ± 0.05	-1.71
6718.130	33557.951	ev	6.5	18676.965	od	6.5	1.45 ± 0.23	-0.86
6727.816	26351.767	ev	4.5	11492.204	od	5.5	0.31 ± 0.04	-1.67
6752.649	33557.951	ev	6.5	18753.034	od	7.5	6.5 ± 1.2	-0.21
6753.889	34900.473	od	3.5	20098.274	ev	3.5	2.8 ± 0.3	-0.81
6765.498	34178.776	ev	5.5	19401.977	od	4.5	0.36 ± 0.08	-1.53
6786.313	34108.475	od	4.5	19376.999	ev	4.5	2.8 ± 0.3	-0.71
6813.179	32490.510	ev	3.5	17817.123	od	4.5	0.26 ± 0.04	-1.85
6834.806	32946.196	ev	5.5	18319.239	od	4.5	0.44 ± 0.07	-1.44
6846.569	25668.692	ev	3.5	11066.865	od	4.5	1.36 ± 0.16	-1.11
6857.121	32304.409	ev	4.5	17725.052	od	5.5	3.3 ± 0.5	-0.63
6884.359	27297.741	ev	2.5	12776.067	od	2.5	0.095 ± 0.014	-2.39
6887.583	34608.122	od	5.5	20093.245	ev	5.5	2.28 ± 0.28	-0.71
6900.700	32304.409	ev	4.5	17817.123	od	4.5	1.23 ± 0.20	-1.06
6919.575	35605.266	od	5.5	21157.496	ev	6.5	0.71 ± 0.10	-1.21
6920.583	32262.787	ev	3.5	17817.123	od	4.5	1.9 ± 0.3	-0.97
6945.035	32490.510	ev	3.5	18095.705	od	2.5	0.34 ± 0.07	-1.71
6945.950	32262.787	ev	3.5	17869.878	od	3.5	1.55 ± 0.27	-1.05
6947.237	32260.120	ev	2.5	17869.878	od	3.5	0.33 ± 0.06	-1.85

Table 3—Continued

λ_{air} (Å)	E_{upper} (cm^{-1})	Parity	J_{upp}	E_{lower} (cm^{-1})	Parity	J_{low}	A-value (10^6 s^{-1})	$\text{Log}(gf)$
6959.216	32684.712	ev	4.5	18319.239	od	4.5	1.20 ± 0.20	-1.06
6971.640	32490.510	ev	3.5	18150.637	od	3.5	1.22 ± 0.19	-1.15
6978.240	34900.473	od	3.5	20574.163	ev	4.5	1.30 ± 0.16	-1.12
6985.859	32677.540	od	6.5	18366.854	ev	7.5	3.9 ± 0.5	-0.40
6988.714	32946.196	ev	5.5	18641.357	od	5.5	0.92 ± 0.16	-1.09
6996.746	32677.540	od	6.5	18389.122	ev	6.5	4.5 ± 0.6	-0.33
7006.079	34900.473	od	3.5	20631.090	ev	2.5	2.11 ± 0.26	-0.91
7006.154	32946.196	ev	5.5	18676.965	od	6.5	3.4 ± 0.7	-0.52
7037.227	32595.348	od	5.5	18389.122	ev	6.5	2.31 ± 0.29	-0.69
7037.768	35362.630	od	6.5	21157.496	ev	6.5	0.55 ± 0.09	-1.24
7044.983	36723.695	od	5.5	22533.110	ev	5.5	1.62 ± 0.23	-0.84
7050.964	32150.143	ev	2.5	17971.595	od	2.5	2.3 ± 0.4	-1.00
7054.585	32490.510	ev	3.5	18319.239	od	4.5	2.0 ± 0.3	-0.92
7056.671	32262.787	ev	3.5	18095.705	od	2.5	0.30 ± 0.06	-1.75
7058.000	32260.120	ev	2.5	18095.705	od	2.5	1.13 ± 0.18	-1.29
7065.768	32150.143	ev	2.5	18001.302	od	1.5	0.51 ± 0.09	-1.64
7082.684	35272.546	od	7.5	21157.496	ev	6.5	0.20 ± 0.04	-1.62
7084.139	32262.787	ev	3.5	18150.637	od	3.5	0.43 ± 0.08	-1.58
7085.478	32260.120	ev	2.5	18150.637	od	3.5	0.87 ± 0.14	-1.41
7101.706	32048.837	ev	1.5	17971.595	od	2.5	0.80 ± 0.13	-1.61
7109.793	32048.837	ev	1.5	17987.607	od	0.5	0.63 ± 0.11	-1.72
7116.725	32048.837	ev	1.5	18001.302	od	1.5	2.4 ± 0.4	-1.14
7118.843	32684.712	ev	4.5	18641.357	od	5.5	3.3 ± 0.5	-0.60
7133.129	34108.475	od	4.5	20093.245	ev	5.5	1.45 ± 0.19	-0.96
7135.689	34108.475	od	4.5	20098.274	ev	3.5	2.17 ± 0.27	-0.78
7141.141	32150.143	ev	2.5	18150.637	od	3.5	0.86 ± 0.16	-1.40
7146.875	33211.481	ev	3.5	19223.207	od	3.5	0.52 ± 0.12	-1.49
7147.299	32677.540	od	6.5	18690.096	ev	5.5	1.74 ± 0.22	-0.73
7164.258	35111.830	od	6.5	21157.496	ev	6.5	1.02 ± 0.14	-0.96
7172.242	27864.534	ev	5.5	13925.734	od	6.5	0.89 ± 0.12	-1.09
7189.546	32595.348	od	5.5	18690.096	ev	5.5	3.7 ± 0.4	-0.46

Table 3—Continued

λ_{air} (Å)	E_{upper} (cm^{-1})	Parity	J_{upp}	E_{lower} (cm^{-1})	Parity	J_{low}	A-value (10^6 s^{-1})	$\text{Log}(gf)$
7197.029	32260.120	ev	2.5	18369.326	od	1.5	1.56 ± 0.29	-1.14
7220.356	33596.027	ev	4.5	19750.111	od	5.5	0.28 ± 0.07	-1.67
7237.867	31908.123	ev	3.5	18095.705	od	2.5	0.15 ± 0.03	-2.03
7240.267	33557.951	ev	6.5	19750.111	od	5.5	0.18 ± 0.03	-1.70
7252.659	27162.224	ev	4.5	13377.976	od	5.5	0.62 ± 0.09	-1.31
7377.236	36821.816	od	6.5	23270.336	ev	7.5	4.9 ± 0.7	-0.25
7381.191	32946.196	ev	5.5	19401.977	od	4.5	0.20 ± 0.04	-1.70
7385.967	32490.510	ev	3.5	18955.050	od	2.5	1.24 ± 0.20	-1.09
7394.866	26595.222	ev	3.5	13076.050	od	4.5	0.49 ± 0.07	-1.49
7426.544	32684.712	ev	4.5	19223.207	od	3.5	0.71 ± 0.12	-1.23
7432.551	34608.122	od	5.5	21157.496	ev	6.5	1.00 ± 0.13	-1.00
7505.317	26211.912	ev	2.5	12891.692	od	3.5	0.32 ± 0.04	-1.80
7526.498	32684.712	ev	4.5	19401.977	od	4.5	0.35 ± 0.06	-1.52
7563.159	32595.348	od	5.5	19376.999	ev	4.5	1.98 ± 0.27	-0.69
7576.489	32150.143	ev	2.5	18955.050	od	2.5	0.142 ± 0.026	-2.14
7644.635	26455.446	ev	4.5	13377.976	od	5.5	0.074 ± 0.013	-2.19
7647.742	35605.266	od	5.5	22533.110	ev	5.5	0.16 ± 0.03	-1.78
7748.345	32304.409	ev	4.5	19401.977	od	4.5	0.46 ± 0.08	-1.38
7773.421	32262.787	ev	3.5	19401.977	od	4.5	0.19 ± 0.04	-1.87
7778.969	36821.816	od	6.5	23970.178	ev	6.5	0.61 ± 0.10	-1.11
7787.191	34900.473	od	3.5	22062.405	ev	2.5	1.8 ± 0.3	-0.88
7838.818	36723.695	od	5.5	23970.178	ev	6.5	2.0 ± 0.3	-0.65
7844.947	34108.475	od	4.5	21364.923	ev	3.5	1.24 ± 0.17	-0.94
7846.361	35272.546	od	7.5	22531.290	ev	8.5	9.7 ± 1.5	0.16
7881.211	31908.123	ev	3.5	19223.207	od	3.5	0.141 ± 0.029	-1.98
7963.209	32304.409	ev	4.5	19750.111	od	5.5	0.93 ± 0.16	-1.05
7996.455	32595.348	od	5.5	20093.245	ev	5.5	0.140 ± 0.023	-1.79
8160.781	36778.403	od	4.5	24528.042	ev	5.5	1.00 ± 0.17	-1.00
8165.143	30996.851	ev	6.5	18753.034	od	7.5	0.16 ± 0.03	-1.64
8184.109	32262.787	ev	3.5	20047.344	od	3.5	0.116 ± 0.024	-2.03
8267.457	35362.630	od	6.5	23270.336	ev	7.5	0.61 ± 0.11	-1.06

Table 3—Continued

λ_{air} (Å)	E_{upper} (cm ⁻¹)	Parity	J_{upp}	E_{lower} (cm ⁻¹)	Parity	J_{low}	A-value (10 ⁶ s ⁻¹)	Log(gf)
8329.510	35272.546	od	7.5	23270.336	ev	7.5	0.20 ± 0.04	-1.47
8418.604	34900.473	od	3.5	23025.282	ev	4.5	0.48 ± 0.08	-1.39
8442.561	35111.830	od	6.5	23270.336	ev	7.5	1.24 ± 0.19	-0.73
8598.722	30849.648	ev	4.5	19223.207	od	3.5	0.28 ± 0.05	-1.51
8678.139	32677.540	od	6.5	21157.496	ev	6.5	0.196 ± 0.028	-1.51
8733.003	30849.648	ev	4.5	19401.977	od	4.5	0.141 ± 0.026	-1.79
8750.235	29242.250	ev	3.5	17817.123	od	4.5	0.111 ± 0.021	-1.99
8815.868	36778.403	od	4.5	25438.335	ev	4.5	0.68 ± 0.12	-1.10
8825.253	29197.887	ev	2.5	17869.878	od	3.5	0.28 ± 0.05	-1.71
8831.311	29045.291	ev	4.5	17725.052	od	5.5	0.111 ± 0.020	-1.89
8858.605	36723.695	od	5.5	25438.335	ev	4.5	0.31 ± 0.06	-1.36
8994.668	36723.695	od	5.5	25609.049	ev	4.5	0.19 ± 0.03	-1.57
9232.304	29197.887	ev	2.5	18369.326	od	1.5	0.30 ± 0.06	-1.63
9431.099	29353.344	ev	6.5	18753.034	od	7.5	0.21 ± 0.05	-1.40
9445.822	35111.830	od	6.5	24528.042	ev	5.5	0.097 ± 0.019	-1.74
9912.513	35362.630	od	6.5	25277.136	ev	6.5	0.44 ± 0.08	-1.05
9914.145	36723.695	od	5.5	26639.861	ev	5.5	0.71 ± 0.12	-0.90
9949.303	34900.473	od	3.5	24852.273	ev	4.5	0.167 ± 0.029	-1.70
10022.637	29197.887	ev	2.5	19223.207	od	3.5	0.089 ± 0.021	-2.09
10139.137	35362.630	od	6.5	25502.560	ev	7.5	0.77 ± 0.16	-0.78
10339.674	27988.074	ev	3.5	18319.239	od	4.5	0.19 ± 0.04	-1.62
10403.767	35111.830	od	6.5	25502.560	ev	7.5	0.82 ± 0.16	-0.73

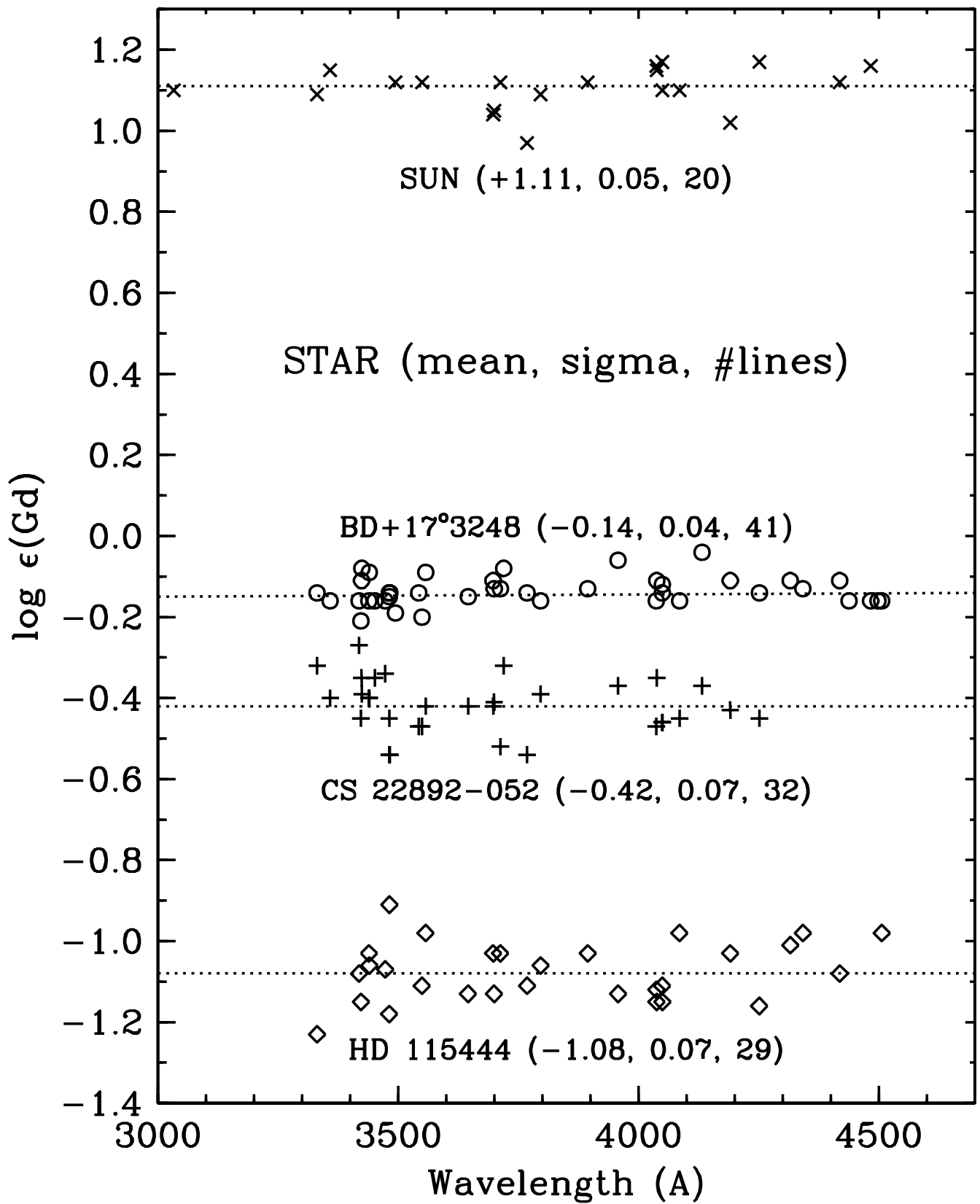
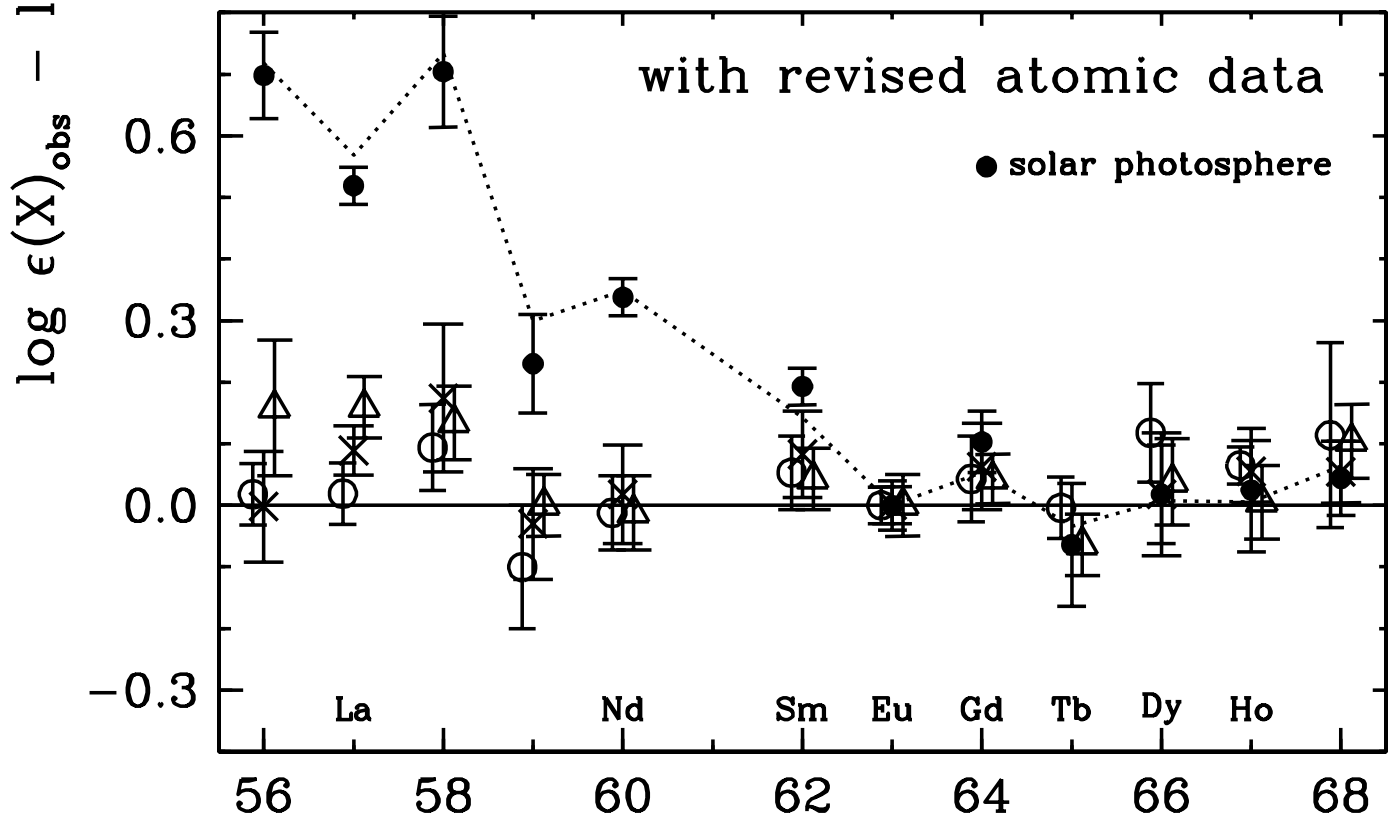
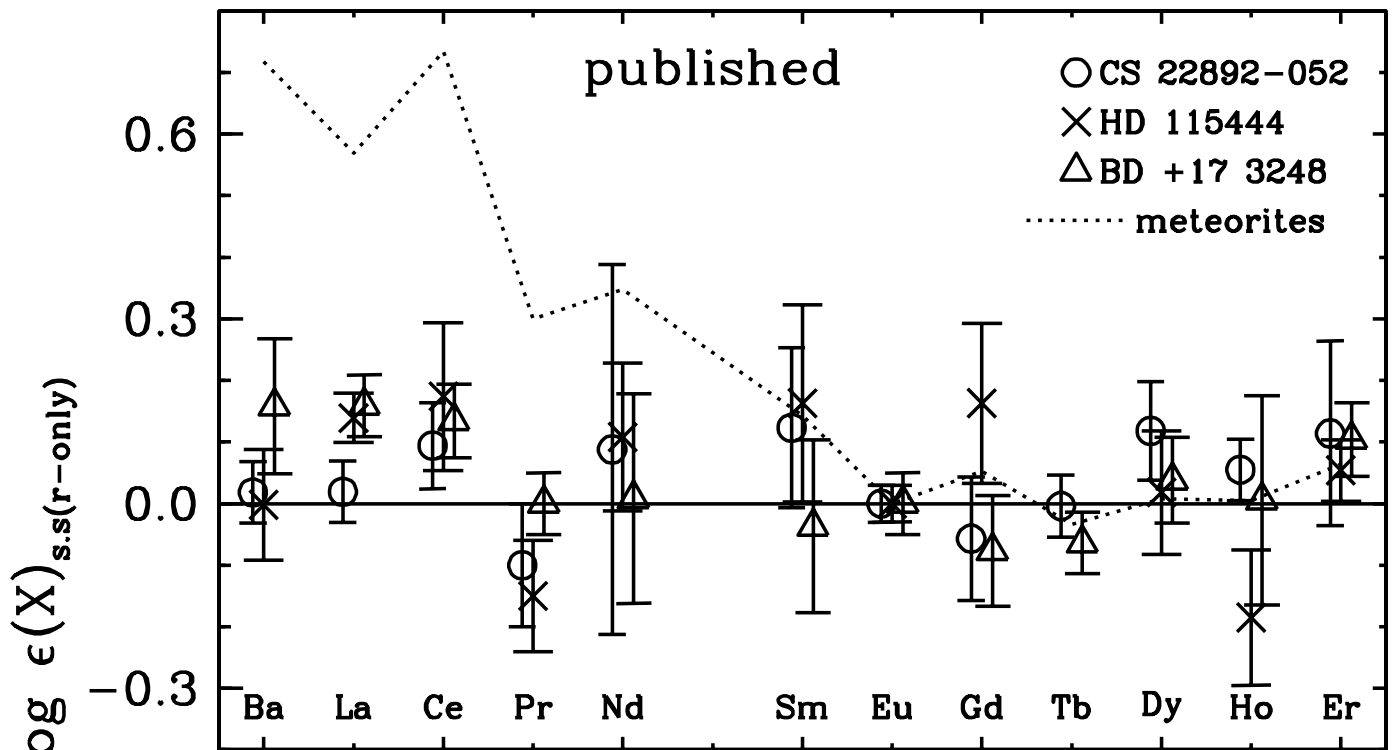


Table 4. Gadolinium abundances from individual lines in the Sun and the r -process-rich metal-poor giant stars. Mean Gd and Eu abundances in the Sun and the same stars.

Lambda	E.P.	Log(gf)	ε_{Sun}	ε_{BD}	ε_{CS}	ε_{HD}
(Å)	(eV)					
3032.844	0.078	0.30	1.10			
3331.387	0.000	-0.28	1.09	-0.14	-0.32	-1.23
3358.625	0.032	0.25	1.15	-0.16	-0.40	
3418.729	0.000	-0.36		-0.16	-0.27	-1.08
3422.464	0.240	0.71		-0.21	-0.45	-1.15
3423.924	0.000	-0.55		-0.11	-0.35	
3424.595	0.354	-0.34		-0.08	-0.39	
3439.208	0.382	0.08		-0.16	-0.40	-1.03
3439.988	0.240	0.21		-0.09	-0.40	-1.06
3451.236	0.382	-0.25		-0.16	-0.35	
3473.224	0.032	-0.37		-0.16	-0.34	-1.07
3481.280	0.600	0.42		-0.14	-0.45	-1.18
3481.802	0.492	0.12		-0.15	-0.54	-0.91
3482.607	0.427	-0.47		-0.14	-0.54	
3494.406	0.078	-0.20	1.12	-0.19		
3542.765	0.662	-0.24		-0.14	-0.47	
3549.359	0.240	0.29	1.12	-0.20	-0.47	-1.11
3557.058	0.600	0.04		-0.09	-0.42	-0.98
3645.618	0.425	-0.38		-0.15	-0.42	-1.13
3697.733	0.032	-0.34	1.04	-0.11	-0.42	-1.03
3699.737	0.354	-0.29	1.05	-0.13	-0.41	-1.13
3712.704	0.382	0.04	1.12	-0.13	-0.52	-1.03
3719.452	1.232	0.46		-0.08	-0.32	
3719.529	0.492	-0.50				
3768.396	0.078	0.21	0.97	-0.14	-0.54	-1.11
3796.384	0.032	0.02	1.09	-0.16	-0.39	-1.06
3894.693	0.000	-0.58	1.12	-0.13		-1.03
3957.667	0.600	-0.25		-0.06	-0.37	-1.13
4037.323	0.662	-0.11	1.16	-0.16	-0.47	-1.12
4037.893	0.556	-0.42	1.15	-0.11	-0.35	-1.15
4049.423	0.662	-0.08	1.17	-0.14	-0.46	-1.11

Table 4—Continued

Lambda	E.P.	Log(<i>gf</i>)	ε_{Sun}	ε_{BD}	ε_{CS}	ε_{HD}
(Å)	(eV)					
4049.854	0.990	0.49	1.10	-0.12	-0.46	-1.15
4085.558	0.731	-0.01	1.10	-0.16	-0.45	-0.98
4132.264	0.601	-0.15		-0.04	-0.37	
4191.075	0.427	-0.48	1.02	-0.11	-0.43	-1.03
4251.731	0.382	-0.22	1.17	-0.14	-0.45	-1.16
4316.047	0.662	-0.45		-0.11		-1.01
4342.181	0.600	-0.27		-0.13		-0.98
4419.029	0.492	-0.70	1.12	-0.11		-1.08
4438.254	0.662	-0.82		-0.16		
4483.329	1.059	-0.42	1.16	-0.16		
4498.286	0.427	-1.08		-0.16		
4506.337	0.499	-1.03		-0.16		-0.98
5733.852	1.371	-0.65	1.15			
Gd: mean			1.11	-0.14	-0.42	-1.08
±			0.01	0.01	0.01	0.01
Gd: σ			0.05	0.04	0.07	0.07
Gd: number			20	41	32	29
Eu: mean			0.52	-0.67	-0.95	-1.64
±			0.01	0.02	0.01	0.01
Gd: σ			0.04	0.05	0.03	0.02
Eu: number			14	9	8	5
Gd-Eu			0.59	0.53	0.53	0.56



Atomic Number

Table 5. Predicted Solar r-Process Elemental Abundances

Element	N_s^a	N_r^a	$\langle \text{el-Eu} \rangle$	$N_r(\text{predicted})^b$	Total Solar ^c	$\log \epsilon_{total}^c$
Gd	0.062	0.276	0.54	0.312	0.374	1.11
Sm	0.086	0.174	0.353	0.203	0.289	1.00
Nd	0.484	0.352	0.593	0.353	0.837	1.46
Ho	0.006	0.083	0.007	0.091	0.097	0.53

Note. — ^aOriginal prediction (based upon Ni = 10⁶ scale) from Käppeler *et al.* (1989), Simmerer *et al.* (2004); Cowan *et al.* (2006).

^bBased upon average $\langle \text{el-Eu} \rangle$ for CS 22892-052, HD 115444 and BD +17°3248.

^c $N_{total} = N_s + N_r(\text{predicted})$

Table 6. Contributions of Gd from the s- and r-processes based on the $\text{Si} = 10^6$ scale.

Isotope	s-abundance ^a	%	r-abundance ^a	%	s-abundance ^b	%	r-abundance ^b	%
¹⁵² Gd ^c	0.001	1.6	0.0	0.0	0.001	1.8	0.0	0.0
¹⁵⁴ Gd ^c	0.009	14.5	0.0	0.0	0.007	12.8	0.0	0.0
¹⁵⁵ Gd	0.003	4.8	0.048	16.3	0.004	7.3	0.046	16.5
¹⁵⁶ Gd	0.015	24.2	0.055	19.9	0.0125	22.9	0.056	20.1
¹⁵⁷ Gd	0.007	11.3	0.046	16.7	0.006	11.0	0.046	16.5
¹⁵⁸ Gd	0.027	43.5	0.058	21.0	0.023	42.2	0.06	21.5
¹⁶⁰ Gd	0	0	0.072	26.1	0.001	1.8	0.071	25.4

Note. — ^aStandard Model: Käppeler *et al.* (1989), Simmerer *et al.* (2004); Cowan *et al.* (2006).

^bStellar Model: Arlandini *et al.* (1989).

^cOnly s-process.